Carbon Dioxide Utilisation—The Formate Route

Luisa B. Maia, Isabel Moura, and José J. G. Moura

Abstract

The relentless rise of atmospheric CO_2 is causing large and unpredictable impacts on the Earth climate, due to the CO_2 significant greenhouse effect, besides being responsible for the ocean acidification, with consequent huge impacts in our daily lives and in all forms of life. To stop spiral of destruction, we must actively reduce the CO_2 emissions and develop new and more efficient "CO_2 sinks". We should be focused on the opportunities provided by exploiting this novel and huge carbon feedstock to produce de novo fuels and added-value compounds. The conversion of CO_2 into formate offers key advantages for carbon recycling, and formate dehydrogenase (FDH) enzymes are at the centre of intense research, due to the "green" advantages the bioconversion can offer, namely substrate and product selectivity and specificity, in reactions run at ambient temperature and pressure and neutral pH. In this chapter, we describe the remarkable recent progress towards efficient and selective FDH-catalysed CO_2 reduction to formate. We focus on the enzymes, discussing their structure and mechanism of action. Selected promising studies and successful proof of concepts of FDH-dependent CO_2 reduction to formate and beyond are discussed, to highlight the power of FDHs and the challenges this CO_2 bioconversion still faces.

Keywords

Carbon dioxide utilisation · Formic acid · Formate dehydrogenase · Molybdenum · Tungsten · Hydride transfer · Biocatalyst · Green chemistry · Energy · Biotechnology

L. B. Maia (✉) · I. Moura · J. J. G. Moura
LAQV, REQUIMTE, NOVA School of Science and Technology, Campus de Caparica, Caparica, Portugal
e-mail: luisa.maia@fct.unl.pt

J. J. G. Moura et al. (eds.), *Enzymes for Solving Humankind's Problems*,
https://doi.org/10.1007/978-3-030-58315-6_2

Abbreviations

CCS	Carbon dioxide capture and sequestration
Cys-Mo-FDH	Cysteine, molybdenum-containing formate dehydrogenase
Cys-W-FDH	Cysteine, tungsten-containing formate dehydrogenase
EPR	Electron paramagnetic resonance spectroscopic
Fe/Fe-Hase	Iron–iron hydrogenase
Fe/S	Iron–sulfur centres
FDH	Formate dehydrogenase
FMFDH	*N*-formyl-methanofuran dehydrogenase
GDE	Gas diffusion electrode
Mo-FDH	Molybdenum-containing formate dehydrogenase
Ni/Fe-Hase	Nickel/iron-containing hydrogenase
RES	Renewable energy sources
SeCys-Mo-FDH	Selenocysteine, molybdenum-containing formate dehydrogenase
SeCys-W-FDH	Selenocysteine, tungsten-containing formate dehydrogenase
XAS	X-ray absorption spectroscopy
VC	Added-value compounds or valuable compounds
W-FDH	Tungsten-containing formate dehydrogenase

1 The Relentless Rise of Carbon Dioxide

In 2018 alone, more than 36Gt of CO_2 [1] were dumped into the atmosphere as waste material from fossil resources-based energy and chemical industries! In that year, the global atmospheric CO_2 concentration reached an annual average value of 407 ppm, an increase of 150% since pre-industrial times (277 ppm in 1750) (Fig. 1) [1]. Yet, new records are being set, and a monthly average of 416 ppm was already observed this March 2020 [2]. This ever-increasing atmospheric CO_2 concentration is causing large and unpredictable impacts on the Earth climate, due to the CO_2 significant greenhouse effect, besides being responsible for the ocean acidification, with consequent huge impacts in our daily lives and in all forms of life.

Atmospheric CO_2 concentration results from the balance between CO_2 emission and uptake [3]. CO_2 is emitted from human activities, such as fossil fuel combustion and oxidation from other energy and industrial processes (10.0Gt of carbon in 2018 [1]) and deliberate activities on land, mainly deforestation (1.5Gt of carbon in 2018 [1]), as well as, from natural processes, such as volcanic eruptions and biological emissions. On the other plate of the scale, the small "CO_2 sinks" are mainly provided by physical and biological processes in oceans (2.6Gt of carbon in

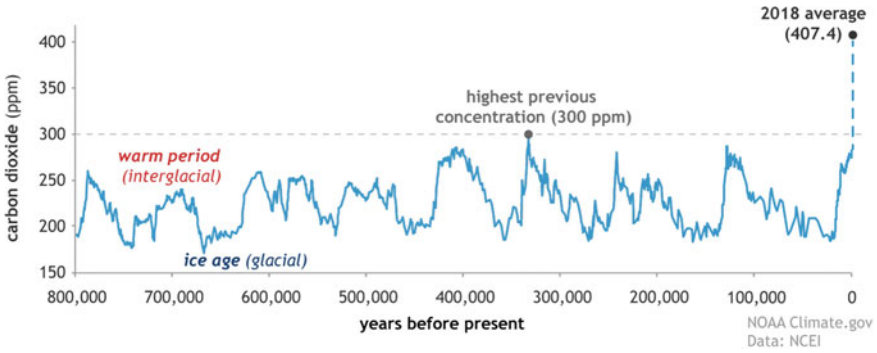

Fig. 1 Relentless rise of carbon dioxide. Global atmospheric CO_2 concentrations in parts per million (ppm) for the past 800,000 years. The peaks and valleys track ice ages (low CO_2) and warmer interglacials (higher CO_2). During these cycles, CO_2 was never higher than 300 ppm. In 2018, it reached 407.4 ppm. On the geologic time scale, the increase (blue dashed line) looks virtually instantaneous *Source* NOAA Climate.gov, based on EPICA Dome C data provided by NOAA NCEI Paleoclimatology Program (https://www.climate.gov/news-features/understanding-climate/climate-change-atmospheric-carbon-dioxide)

2018 [1]) and land (3.5Gt of carbon in 2018 [1]). To break this largely unfavourable imbalance (more than 5Gt in 2018), we must actively reduce the CO_2 emissions and develop new and more efficient "CO_2 sinks"—new individual actions and political decisions are needed, as reviewed by Seixas and Ferreira in this book [3].

Until recently, the debate often focused only on "passive CO_2 mitigation", searching for strategies for CO_2 capture and sequestration (CCS). Instead, we should be looking at the opportunities for the energy and chemical industries provided by exploiting this novel and huge carbon feedstock (Fig. 2), such as (a) storage of "intermittent" renewable energy sources (RES) (wind, solar and hydropower energy, which are now rapidly growing and becoming economically viable), (b) conversion of RES-derived electricity into fuels (mainly for mobility and transport sector, in particular aviation and heavy freight over long distances, the major polluters), (c) production of added-value compounds (VC) and feedstock chemicals for making all the modern-world chemical commodities (from bulk chemicals to plastics, fertilisers and even pharmaceuticals). Regarding atmospheric CO_2 reduction, points (a) and (b) (energy industry) are of major relevance, as the different scales of energy and chemical industries impede the VC production to function as a quantitative "sink" for the massive fossil fuels-dependent CO_2 emissions. Together, these three axes, storage/conversion/production, will certainly provide a straightforward way to actively reduce the CO_2 emissions, while actively consuming the CO_2 already released—"two-in-one solution".

But, how to direct CO_2 into the storage/conversion/production axes? Formic acid/formate[1] offers key advantages (Fig. 2)!

[1] pK_{a1} (formic acid (methanoic acid, HCOOH)/formate) = 3.77.

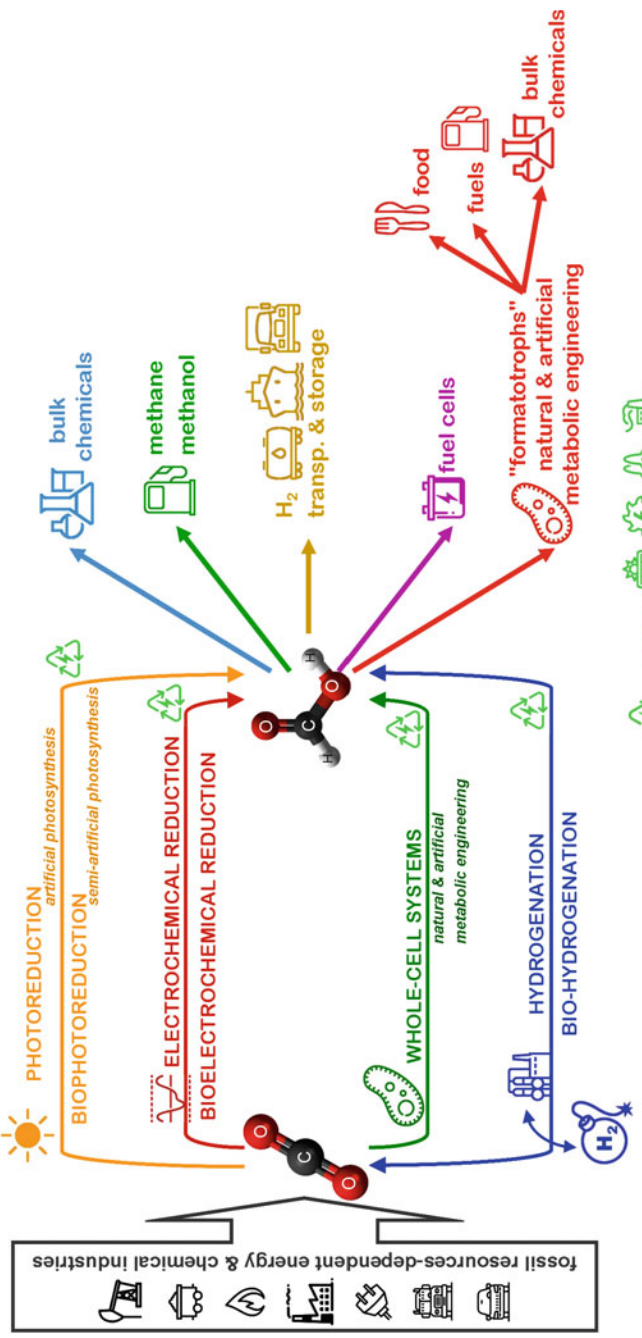

Fig. 2 Directing CO_2 into the axes storage/conversion/production through the formate route. (icons from www.icons8.com)

2 Formic Acid—The Stepping Stone Towards Carbon Dioxide Utilisation

Formic acid was identified in fifteenth century as an acidic vapour in ant hills, from where its name derivates—"formica", the Latin word for ant. It was first synthesised only in the nineteenth century from hydrocyanic acid by the famous French chemist and physicist Joseph Gay-Lussac and also from carbon monoxide by another French chemist, Marcellin Berthelot. However, formic acid received little industrial attention until the last quarter of twentieth century, when it started to be used as a preservative and antibacterial in livestock feed due to its low toxicity (LD_{50} of 1.8 g/kg). More recently, formic acid regained a new interest, due to some features that are key to the longed-for "post-fossil era" (Fig. 2).

(a) Formic acid is a stable product that can be formed by the "simple" two-electron reduction of CO_2 (Eq. 1), what, noteworthy, resulted in a considerable attention to the electrochemical CO_2 reduction in the last decade (see Sect. 3.).
(b) Besides formic acid, also carbon monoxide is a stable product of the two-electron CO_2 reduction (Eq. 2). However, its high toxicity, low solubility and low mass transfer rate make the carbon monoxide subsequent utilisation challenging. In contrast, formic acid is a highly soluble and stable liquid, easy to store and transport.
(c) Formic acid is also not explosive, what represents an important advantage relatively to dihydrogen, an ideal "clean" fuel (see below).
(d) Formic acid is already used as a "building block" in chemical industry.
(e) Formic acid can be a substrate for further reduction to a carbon-based fuel, methanol and methane, what might not be the most obvious option regarding CO_2 consumption.
(f) Formic acid, formed from CO_2 and dihydrogen (Eq. 3), can be used as a "storage form" of dihydrogen, an ideal "clean" fuel (potentially zero contribution to the global carbon cycle, with a high gravimetric energy density) [4–13]. Although formic acid is not a perfect dihydrogen "storage medium", due to its relatively small hydrogen content (4.4%(m/m) or 5.3%(m/v)), it is currently still one of the best options to circumvent the technical difficulties associated with dihydrogen handling, storage and transport. For this purpose, formic acid produced by CO_2 hydrogenation or any other approach is converted back to dihydrogen when needed.
(g) Moreover, formic acid fuel cells are being the centre of a renewed interest [14–18].
(h) From a biotechnological point of view, formate can be both produced and assimilated by many natural and biotechnologically engineered organisms and, unlike dihydrogen (that is "just" oxidised to form reducing power), act as a carbon source for "formatotrophic" organisms, thus, enabling considerably higher biomass formation and VC and fuels production yields [19].

$$CO_2 + 2e^- + 2H^+ \rightleftharpoons HCOOH \quad (1)$$

$$CO_2 + 2e^- + 2H^+ \rightleftharpoons CO + H_2O \quad (2)$$

$$CO_2 + H_2 \rightleftharpoons HCOOH \quad (3)$$

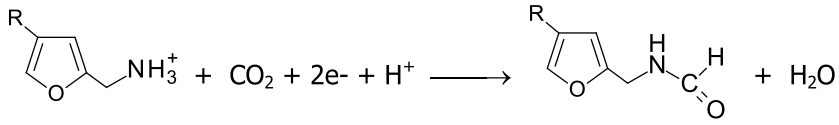

methanofuran formyl-methanofuran (4)

3 How to Convert Carbon Dioxide to Formic Acid/Formate?—The Chemical Way

CO_2 is a kinetically and thermodynamically stable molecule, with a high negative value of the reduction potential of the CO_2/HCOOH pair (highly pH dependent), what makes its activation and reduction a difficult task [8]. Hence, perhaps the first answer that comes to mind to reduce CO_2 to formate is: electrochemically [20–33]. However, the feasibility—meaning essentially the economic viability—of this process, that is currently the centre of intense research, depends on the Faradaic efficiency and energetic efficiency of CO_2 reduction (avoiding high electrochemical overpotentials) and on the rate and selectivity (purity) of formate production. The other "cost" to be considered is obviously the environmental one, and this depends on the use of a RES-derived electricity and on the sustainability of the electrodes (composition and durability).

The second answer is probably going to be photoreduction, which is the most straightforward way to use a RES to convert CO_2. Solar energy (photogenerated electrons) can be used to drive chemical reactions, and this solar-to-chemical energy conversion followed by storage in the form of chemical bonds is generally called "artificial photosynthesis" (as it is a mimic of photosynthetic process used by living organism to fix CO_2). The progress in this field has been quite remarkable, and several highly efficient and promising systems have been developed for CO_2 reduction (as well as water oxidation and hydrogen evolution), and formic acid can be produced with high rates and selectivity [34–44]. However, some problems have yet to be solved. In a very simplified way, artificial photosynthesis needs two fundamental components: an ideal light absorber/photosensitiser (for light harvest, charge separation and charge transfer) and an ideal catalyst (with high intrinsic activity and stability and low overpotential). Therefore, the heterogenisation of the molecular catalysts and engineering of applicable devices are the main challenges towards the development of effective artificial photosynthesis devices (practical

problems, such as density and exposure of the catalyst active sites, conductivity, mass transport and stability of the catalyst-derived material or electrode, all make the catalyst intrinsic activity and efficiency quite different from the device performance numbers). In addition, scale-up feasibility and whole device long-term stability (also associated with the costs of using expensive high-purity semiconductors to achieve high efficiency) have to be attained. Nevertheless, artificial photosynthesis devices might become economically viable sooner than many anticipate: considering the energy consumption forecasted for 2050, the future solar energy devices only need a ≈ 10% solar-to-fuel efficiency (already achievable in proof of concept devices!) if 1% of the Earth's surface is covered [44].

Formic acid can also be produced chemically from CO_2 and dihydrogen. This CO_2 hydrogenation is just the thermal overall CO_2 reduction by dihydrogen using molecular catalysts (Eq. 3), as an alternative to direct electrochemical or photoelectrochemical reduction of CO_2 [5, 10, 12, 13, 45–71]. Hence, here, it is the rational design of the catalytic systems (efficiency and selectivity) that must be attained and the systems that have been developed to date exhibit selectivity and yield lower than desirable, besides requiring a high temperature and/or high pressure. Dihydrogen is a "clean" fuel (potentially zero contribution to the global carbon cycle), but its real environmental impact depends on how it is produce. The industrial production of dihydrogen (primarily from methane) requires harsh temperatures and emits as much CO_2 into the atmosphere as natural gas burning [72]. To be environmentally friendly, dihydrogen must be produced by electrolysis of water using a RES and selected heterogeneous or homogeneous catalysts or biological systems [73–93]. As noted above, besides producing formic acid itself, CO_2 hydrogenation is thought as a relevant way to storage dihydrogen. Therefore, also the reversible interconversion of formic acid to CO_2 and dihydrogen must be carefully considered.

4 How to Convert Carbon Dioxide to Formic Acid/Formate?—Exploiting the Power of Formate Dehydrogenases (Enzymes for Solving Humankind's Problems)

4.1 The Biochemical Way

In contrast to purely physicochemical, biological processes are substrate and product-specific (life requires a well-defined metabolism) and occur under truly "green", sustainable conditions, at ambient temperature and pressure and close to neutral pH. Biological catalysts—enzymes—offer selectivity and specificity, coupled with high specific activity (in terms of active sites) and maximal rate (under the respective cellular context). Enzymes have evolved to become perfect catalysts[2],

[2]It should be kept in mind that enzymes did not evolve to maximise "our" VC production. Enzymes and all cellular components evolved to achieve sustained life. The statement of "perfect catalysts" must be taken within the respective context.

comprising (a) *specific* surface patches to establish contact with *specific* biomolecules (for cell localisation, integration into metabolic complexes, crosstalk or simple electron transfer), (b) channels where only (or mainly) the *correct* substrates come in and well-determined products come out, as well as, (c) highly defined active sites, assembled to promote the formation of key transition states and intermediates and, thus, lower the reaction energy barriers and energy loss. For that, active sites are built with precise steric features, electrostatic and hydrogen bonding interactions, fine-tuned reduction potentials and pK_a values and optimised (and often synchronised) electron and proton transfer paths. The power and efficiency of biological catalysis is such that enzymes cascades are the cornerstone of all metabolic pathways that sustain life on Earth. Hence, there is a growing interest in making use of all the advantages the "biochemical way" can provide. Numerous hybrid systems have been (are being) designed to merge the best of the two worlds —chemical and biochemical—and the CO_2 reduction to formate is no exception.

4.2 Formate Dehydrogenases—Enzymatic Machineries

To interconvert CO_2 and formate, living organisms use formate dehydrogenase (FDH) enzymes. FDHs are a heterogeneous and broadly distributed group of enzymes that catalyse the reversible two-electron interconversion of formate and CO_2 (Eq. 1) [94–101]. These enzymes evolved to take part in diverse metabolic pathways, being used by some prokaryotic organism to fix (reduce) CO_2 into formate, while other prokaryotes use FDHs to derive energy, by coupling the formate oxidation (which has a very low reduction potential value, $E^{\circ\prime}(CO_2/HCOO^-) = -0.43$ V) to the reduction of several terminal electron acceptors; FDHs are also broadly used by both prokaryotes and eukaryotes in C1 metabolism.

FDHs can be divided into two major classes, based on their cofactor content and the consequent chemical strategy used to carry out the formate/CO_2 interconversion. One class comprises FDHs that have no metal ions or other redox-active centres—*the metal-independent FDHs class* [102–109]. These enzymes are widespread, being found in bacteria, yeasts, fungi and plants, are all (as far as is known) NAD-dependent and belong to the *D*-specific dehydrogenases of 2-oxyacids family. The other class—*the metal-dependent FDHs class* [3]—comprises only prokaryotic enzymes that hold different redox-active centres (Table 1) and whose active site harbours one molybdenum or one tungsten centre (molybdenum-containing FDH (Mo-FDH) or tungsten-containing FDH (W-FDH), respectively) [94–101, 110–112].

[3]It should be noted that the difference between the two FDHs classes is the absence or presence of redox-active centres. All (so far known) metal-independent FDHs are NAD(P)-dependent. In contrast, there are some metal-dependent FDHs that use $NAD(P)^+$/NAD(P)H as a co-substrate, while many other use other physiological redox partners (such as membrane quinols, cytoplasmatic and periplasmatic cytochromes, ferredoxins or coenzyme F_{420}).

Table 1 Summary of the features of some representative formate dehydrogenases and *N*-formyl-methanofuran dehydrogenases

Enzyme	Active site[a]	Subunit composition	Notes
Clostridium carboxidivorans FDH	W SeCys	α W, [4Fe–4S]	• cytoplasmatic? • NAD^+-dependent
Thermoanaerobacter kivui FDH			• hydrogen-dependent CO_2 reductase
Desulfovibrio gigas FDH		αβ α: W, [4Fe–4S] β: 3 [4Fe–4S]	• periplasmatic
Desulfovibrio alaskensis FDH			
Desulfovibrio vulgaris FDH			
Moorella thermoacetica FDH		$(\alpha\beta)_2$ α: W, [4Fe–4S] β: 3 [4Fe–4S]	• cytoplasmatic • $NADP^+$-dependent
Synthrobacter fumaroxidans FDH		$(\alpha\beta\gamma)_2$ W, Fe	• periplasmatic?
Methylobacterium extorquens FDH	W Cys	αβ α: W, ≥ 1 Fe/S β: [4Fe–4S], FMN	• cytoplasmatic • NAD^+-dependent
Escherichia coli FDH H	Mo SeCys	α Mo, [4Fe–4S]	• cytoplasmatic (membrane-bound via its partners) • partner of formate-hydrogen lyase system
Acetobacterium woodii FDH			• hydrogen-dependent CO_2 reductase
Desulfovibrio desulfuricans FDH		αβγ α: Mo, [4Fe–4S] β: 3 [4Fe–4S] γ: 4 *c* haems	• periplasmatic
Desulfovibrio vulgaris FDH			
Escherichia coli FDH N		$(\alpha\beta\gamma)_3$ α: Mo, [4Fe–4S] β: 4 [4Fe–4S] γ: 2 *b* haems	• membrane-bound periplasm-faced • partner in anaerobic nitrate-formate respiratory system
Escherichia coli FDH O			• membrane-bound periplasm-faced • partner in nitrate-formate respiratory system during aerobic to anaerobic transition

(continued)

Table 1 (continued)

Enzyme	Active site[a]	Subunit composition	Notes
Pectobacterium atrosepticum FDH	Mo Cys	α Mo, [4Fe–4S]	• cytoplasmatic
Corynebacterium glutamicum FDH			
Clostridium pasteurianum FDH		αβ Mo, several Fe/S	• cytoplasmatic
Methanobacterium formicicum FDH		αβ Mo, FAD, several Fe/S, Zn	• cytoplasmatic • F_{420}-dependent
Wolinella succinogenes FDH		αβγ α: Mo, [4Fe–4S] β: 4 [4Fe–4S] γ: 4 *b* haems	• membrane-bound
Cupriavidus necator FDH		$(\alpha\beta\gamma)_2$ α: Mo, [2Fe–2S], 4 [4Fe–4S] β: [4Fe–4S], FMN γ: [2Fe–2S]	• cytoplasmatic • NAD^+-dependent
Rhodobacter capsulatus FDH			
Methylosinus trichosporium FDH			
Pseudomonas oxalatus FDH			
Methylosinus trichosporium FDH		$(\alpha\beta\gamma\delta)_2$ Mo, ≥ 1 [2Fe–2S], ≥ 1 [4Fe–4S], FMN	• cytoplasmatic • NAD^+-dependent
Methanothermobacter wolfeiir FMFDH		$(\alpha\beta\gamma\delta\varepsilon\omega)_4$ α: 2 Zn β: Mo, [4Fe–4S] γ: 2 [4Fe–4S] γ: 4 *b* haems δ ε: 8 [4Fe–4S] ω	• cytoplasmatic

[a] Active site composition, besides the two pyranopterin cofactor molecules and the terminal sulfido group

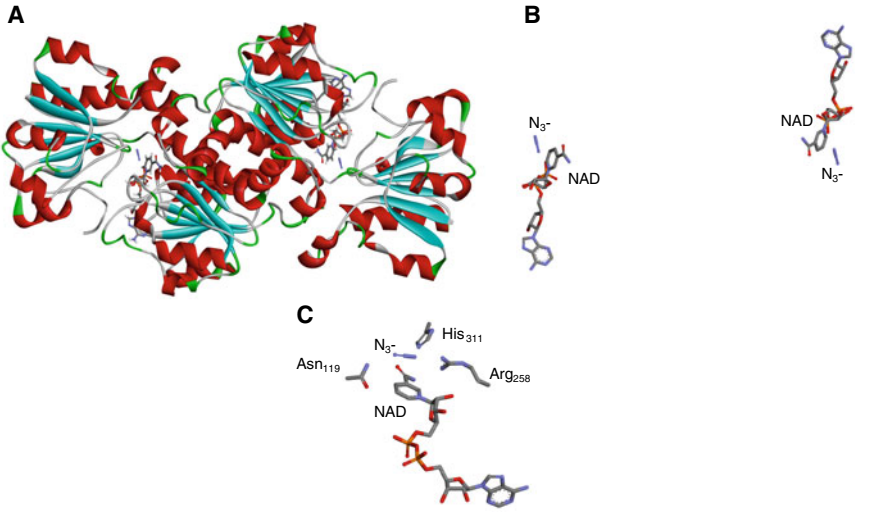

Fig. 3 *C. boidinii* formate dehydrogenase. **A** Three-dimensional structure view of the homodimer. **B** Arrangement of NAD and azide shown in the same orientation (but not same scale) as in (**A**). **C** Enzyme active site, with azide and NAD bound. The structures shown are based on the PDB file 5DN9 [109] (α helices and β sheets are shown in red and cyan, respectively)

4.2.1 The Metal-Independent Formate Dehydrogenases

Comparatively, the metal-independent FDHs are quite simple enzymes, generally forming homodimers, containing a NAD(H) and a formate-binding pockets in a close vicinity of each other (Fig. 3) [102–109]. The formate-binding site harbours a conserved arginine and asparagine residues, while an aspartate and serine residues make contacts to the nicotinamide ring, with another arginine residue binding the phosphate moiety linker of NAD(H).

4.2.2 The Metal-Dependent Formate Dehydrogenases

Because the metal-dependent FDHs are involved in diverse metabolic pathways (energy and C1 metabolism), for which different "interfaces" are needed, this class is extraordinarily heterogeneous, comprising enzymes with diverse redox-active centres, such as iron–sulfur centres (Fe/S), haems and flavins, besides the characteristic molybdenum or tungsten active sites, organised in different subunit compositions and quaternary structures (Table 1) [94–101, 110–112]. This structural diversity is well exemplified by *Escherichia coli*, that expresses one "simple" monomeric cytoplasmatic enzyme, containing only the molybdenum centre and one [4Fe–4S] centre (the FDH H; Fig. 4) [113–117], and two "complex" heteromeric ($(\alpha\beta\gamma)_3$) membrane-bound respiratory enzymes that harbour seven additional redox-active centres ([4Fe–4S] centres and b-type haems) in addition to the molybdenum centre (the FDH N [118–120] (Fig. 5) and FDH O [121–123]). Also, the sulfate-reducing bacteria of the *Desulfovibrio* genus contain diverse Mo-FDHs and W-FDHs [124–129], such as the heterodimeric ($\alpha\beta$) periplasmatic W-FDH of

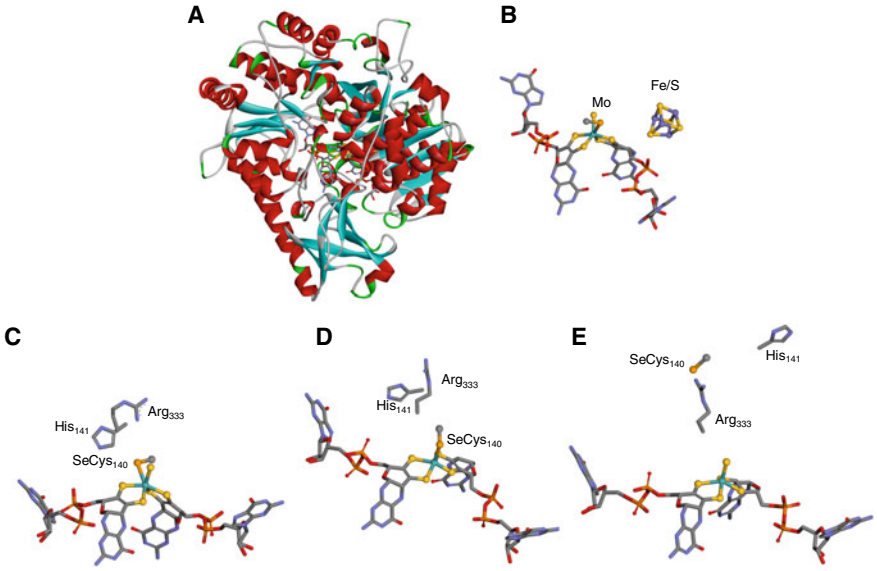

Fig. 4 *E. coli* formate dehydrogenase H. **A** Three-dimensional structure view. **B** Arrangement of the redox-active centres shown in the same orientation (but not same scale) as in (**A**). **C** Molybdenum catalytic centre of oxidised enzyme. **D** Molybdenum catalytic centre of reduced enzyme as suggested by Boyington et al. in 1997 [116]. **E** Molybdenum catalytic centre of reduced enzyme as suggested by Raaijmakers and Romão in 2006 [117]. The structures shown are based on the PDB files 1FDO (**A**, **B**, **C**), 1AA6 (**D**) [116] and 2IV2 (E) [117] (α helices and β sheets are shown in red and cyan, respectively)

D. gigas [130] or *D. vulgaris* [129, 131, 132], with "only" four [4Fe–4S] centres and one tungsten centre (Fig. 6) [133, 134], or the more "complex" heteromeric ($\alpha\beta\gamma$) Mo-FDH of *D. desulfuricans* [135–137] or *D. vulgaris* [129, 131] that contains eight redox-active centres ([4Fe–4S] centres and c-type haems) in addition to the molybdenum centre. Remarkably, the overall protein fold of the molybdenum —and tungsten-containing subunits, including the arrangement of Fe/S centre, is highly conserved[4] [116, 117, 119, 130, 132, 138–140].

The diversity of metal-dependent FDHs is also observed through their "molecular plasticity". Some FDHs take part in formate-hydrogen lyase systems, as is the case of FDH H from *E. coli* (Mo-FDH) [141], *Pectobacterium atrosepticum* (Mo-FDH) [142] or *C. carboxidovorans* (W-FDH) [143–147]. Physiologically, the *E. coli* formate-hydrogen lyase is a membrane-bound system involved in formate

[4]Presently, only five FDHs have been structurally characterised: the *E. coli* Mo-FDHs FDH H [116, 117] and FDH N [119], the *D. gigas* W-FDH [130], the *D. vulgaris* W-FDH [132] and the *Rhodobacter capsulatus* Mo-FDH [138] were crystallographically characterised; the *R. capsulatus* enzyme structure was also determined by cryo-electron microscopy [139]. In addition, also the crystallographic structure of the tungsten-containing *Methanothermobacter wolfeii N*-formyl-methanofuran dehydrogenase, a structurally related enzyme (see below), was solved [140].

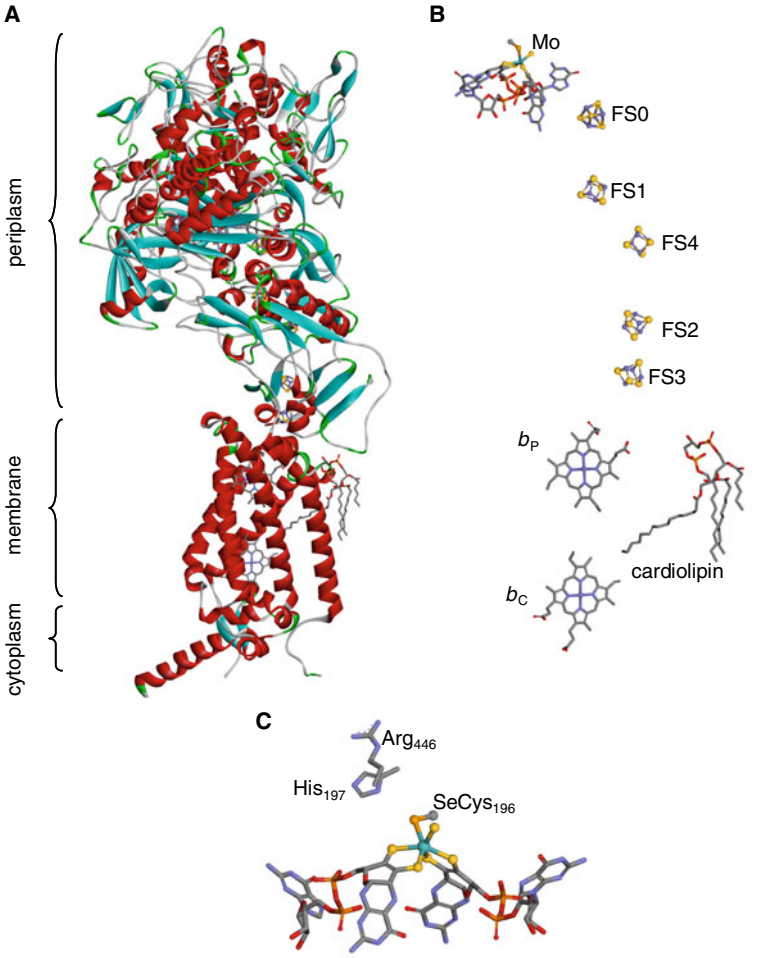

Fig. 5 *E. coli* formate dehydrogenase N. **A** Three-dimensional structure view. **B** Arrangement of the redox-active centres shown in the same orientation (but not same scale) as in (**A**). **C** Molybdenum catalytic centre of oxidised enzyme. The structures shown are based on the PDB file 1KQF [119] (α helices and β sheets are shown in red and cyan, respectively)

oxidation and dihydrogen formation under fermentative growth conditions [141, 148–151]. The system comprises two enzymes, the cytoplasmatic Mo-FDH (described above) and a membrane-bound, cytoplasm-faced nickel/iron-containing hydrogenase (Ni/Fe-Hase); FDH oxidises formate to CO_2 and the resulting reducing equivalents are transferred, through three Fe/S proteins, to the Ni/Fe-Hase that reduces protons to dihydrogen (Fig. 7).

A different rearrangement of the same basic features (FDH plus Hase) is found in cytoplasmatic dihydrogen-dependent FDHs (better denominated as CO_2 reductases), that physiologically catalyse the reduction of CO_2 to formate with the simultaneous

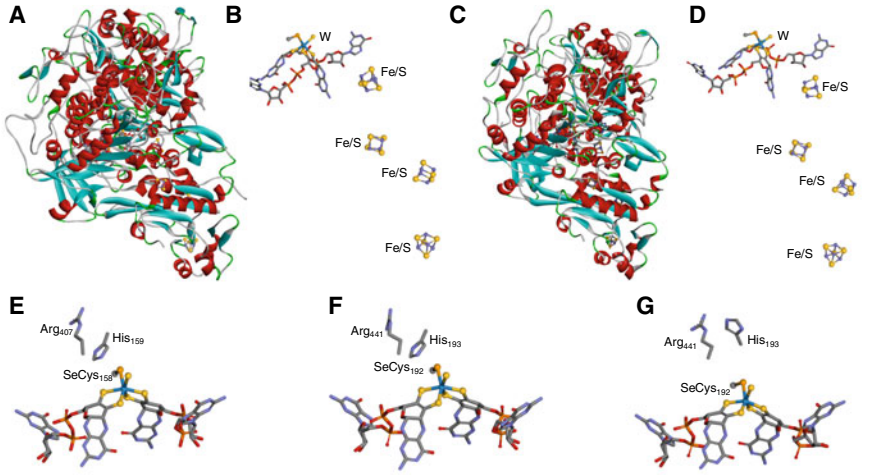

Fig. 6 *D. gigas* (**A**, **B**, **E**) and *D. vulgaris* (**C**, **D**, **F**, **G**) formate dehydrogenases. **A** Three-dimensional structure view of *D. gigas* W-FDH. **B** Arrangement of the redox-active centres of *D. gigas* W-FDH, shown in the same orientation (but not same scale) as in (**A**). **C** Three-dimensional structure view of *D. vulgaris* W-FDH. **D** Arrangement of the redox-active centres of *D. vulgaris* W-FDH, shown in the same orientation (but not same scale) as in (**C**). **E** Tungsten catalytic centre of oxidised *D. gigas* W-FDH. **F** Tungsten catalytic centre of oxidised *D. vulgaris* W-FDH. **G** Tungsten catalytic centre of formate-reduced *D. vulgaris* W-FDH. The structures shown are based on the PDB files 1H0H (**A**, **B**, **E**) [130], 6SDR (**C**, **D**, **F**) and 6SDV (**G**) [132] (α helices and β sheets are shown in red and cyan, respectively)

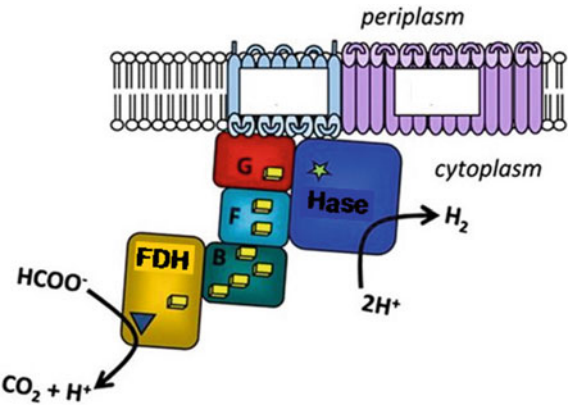

Fig. 7 Predicted architecture of the *E. coli* formate-hydrogen lyase. **B**, **F** and **G** represent three Fe/S proteins. See text for details Adapted with permission from Ref. [149]

and direct oxidation of dihydrogen, that is, without the intervention of an external electron-transfer protein or molecule, as reviewed by Litty and Müller in this Book [152] and also [153–159]. The dihydrogen-dependent CO_2 reductase of the acetogen *A. woodii* is a tetramer ($\alpha\beta\gamma\delta$), holding one FDH-like subunit comprising one molybdenum and one [4Fe–4S] centres, where CO_2 is reduced; the necessary electrons are transferred intramolecularly from an iron–iron hydrogenase-like (Fe/Fe-Hase) subunit (second active site), via two small electron-transfer subunits (each with four [4Fe–4S] centres) (Fig. 8) [153]. A tungsten-containing homologue enzyme is found in *Thermoanaerobacter kivui* [156].

A further example of the "plasticity" of FDH-like proteins is provided by *N*-formyl-methanofuran dehydrogenases (FMFDH) that also have two physically separated active sites: one catalyses the reduction of CO_2 to formate, which is then intramolecularly transferred to the second active site, where it is condensed with methanofuran to form *N*-formyl-methanofuran (Eq. 4) [140, 160, 161]. The FMFDHs are even more complex than FDHs and the enzyme from the methanogen *M. wolfeii* is a tetramer of ($\alpha\beta\gamma\delta\varepsilon\omega$) units, whose CO_2-reducing subunit shares the tungsten and [4Fe–4S] centres, as well as, the protein fold of the W-FDHs and Mo-FDHs (Fig. 9).

In contrast to the structural and organisational diversity, the active site of all presently known metal-dependent FDHs and FMFDH is very well conserved [94–101, 110–112, 140]. In the oxidised form, the active site harbours one molybdenum ion (in the case of Mo-FDHs and Mo-FMFDHs) or one tungsten ion (in W-FDHs and W-FMFDHs) coordinated by the *cis*-dithiolene (–S–C = C–S–) group of two pyranopterin cofactor molecules (Fig. 10), as is characteristic of this family of mononuclear molybdenum and tungsten enzymes [97, 110–112, 162–165]. The metal first coordination sphere is completed by one terminal sulfido group (Mo/W = S)[5] plus one sulfur or selenium atom from a cysteine or selenocysteine residue (Mo/W–S(Cys) or Mo/W–Se(SeCys)) (abbreviated as Cys–Mo–FDH, Cys–W–FDH, SeCys–Mo–FDH and SeCys–W–FDH), in a distorted trigonal prismatic. Noteworthy, there is no apparent relation (as far as is presently known) between the metal and the bound amino acid residue (examples of the four combinations Cys–Mo–FDH, Cys–W–FDH, SeCys–Mo–FDH and SeCys–W–FDH are known for long; Table 1) or the enzyme activity. The active site also comprises two other residues that are strictly conserved to all known FDHs and FMFDHs and are thought to be crucial to the catalytic cycle (as discussed below), one arginine and one histidine (this linked (C-terminal side) to the selenocysteine or cysteine that coordinates the molybdenum or tungsten ion) [116, 117, 119, 130].

[5]Although initially thought to be an oxygen [116], it is now unambiguously established that this terminal atom it is a sulfur, in both Mo-FDHs and W-FDHs, as well as in FMFDH, as established by X-ray crystallography and XAS [117, 140, 166]. In addition, it was already identified the sulfotransferase that, in conjunction with the IscS cysteine desulfurase, catalyses the insertion of this ligand in the active site [167–169].

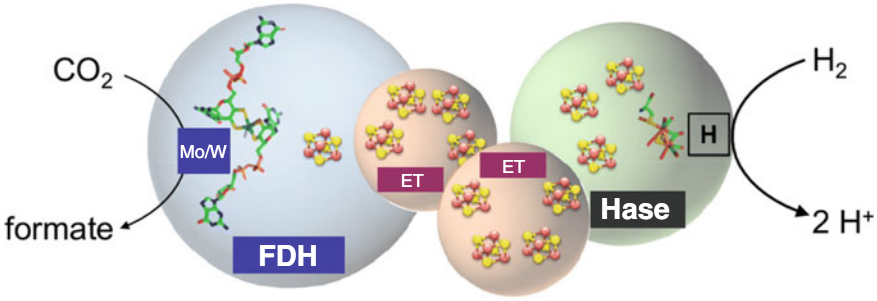

Fig. 8 Structural organisation of *A. woodii* (molybdenum-dependent) and *T. kivui* (tungsten-dependent) dihydrogen-dependent CO_2 reductases. ET represents two small electron-transfer subunits. See text for details Adapted with permission from Ref. [156]. http://creativecommons.org/licenses/by/4.0/

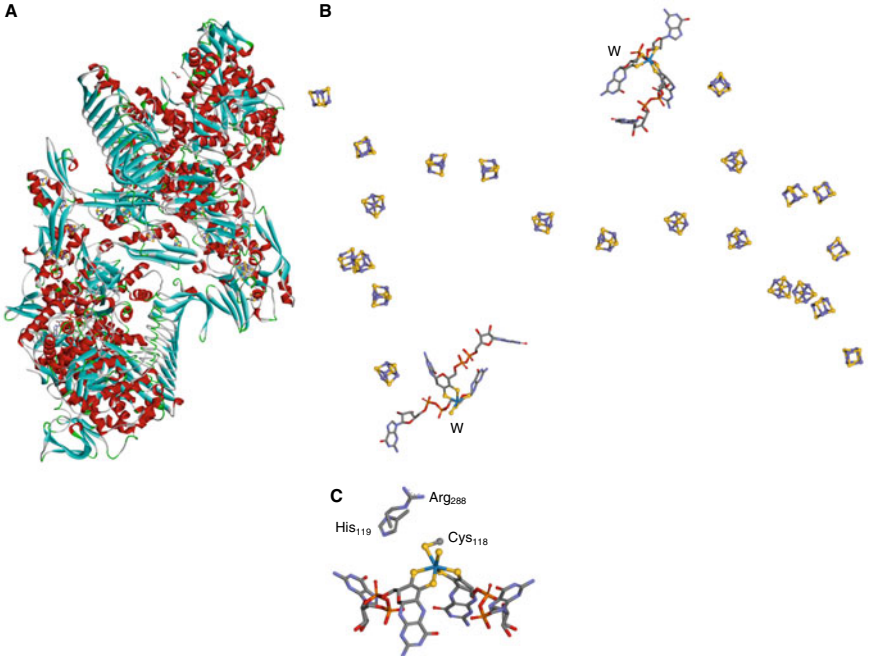

Fig. 9 *M. wolfeii N*-formyl-methanofuran dehydrogenase. **A** Three-dimensional structure view. **B** Arrangement of the redox-active centres shown in the same orientation (but not same scale) as in (**A**). **C** Tungsten catalytic centre of oxidised enzyme. The structures shown are based on the PDB file 5T5I [140] (α helices and β sheets are shown in red and cyan, respectively)

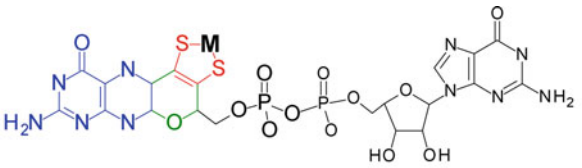

molybdenum/tungten centre in the oxidised state

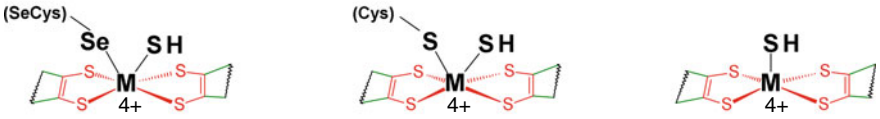

molybdenum/tungten centre in the reduced state

Fig. 10 Active site of formate dehydrogenase and *N*-formyl-methanofuran dehydrogenase. Structure of the pyranopterin cofactor (top). The pyranopterin cofactor molecule is formed by pyrano(green)-pterin(blue)-dithiolene(red)-methylphosphate(black) moieties; in all so far characterised FDHs, the cofactor is found esterified with a guanosine monophosphate (dark grey). The dithiolene (–S–C = C–S–) group forms a five-membered ene-1,2-dithiolene chelate ring with the molybdenum or tungsten ion, here indicated as M (from metal). Structure of the molybdenum/tungsten centre in the oxidised state (middle). For simplicity, only the dithiolene moiety of the pyranopterin cofactor is represented. Structure of the molybdenum/tungsten centre in the reduced state (bottom). For simplicity, only the dithiolene moiety of the pyranopterin cofactor is represented. Contrary to the oxidised state (that is consensually accepted), the structure of the reduced state is still under debate, as discussed below, under Sect. 4.3.2b. The two hypotheses under debate are represented, with the cysteine or selenocysteine residue bound to the metal and with the residue dissociated from the metal (Sect. 4.3.2b)

4.3 Formate Dehydrogenases—Mechanism of Action

4.3.1 The Metal-Independent Formate Dehydrogenases

The metal-independent FDHs are NAD-dependent enzymes, whose chemical strategy to interconvert formate and CO_2 is surprisingly simple and well established (Fig. 11) [102–109]: the enzyme binds formate and NAD^+ in close proximity of each other (1.4 Å distance between H-(formate) and C4-(pyridine ring)) and makes NAD^+ acquire a bipolar conformation, which increases its electrophilicity and, thus, facilitates the hydride transfer. The reaction, then, proceeds by straightforward hydride transfer from formate to NAD^+. In accordance, the rate-limiting step of the

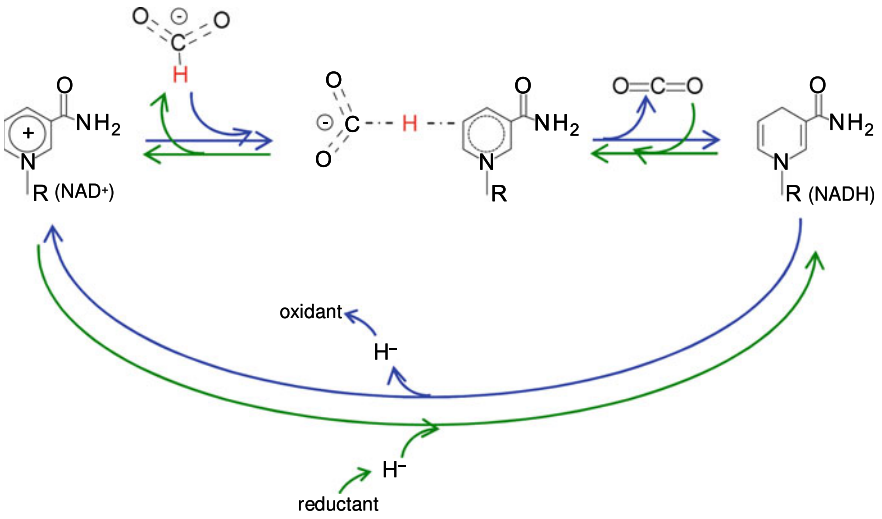

Fig. 11 Hydride transfer mechanism proposed for metal-independent NAD-dependent formate dehydrogenases

catalytic cycle is the formate C–H bond cleavage, as shown by kinetic studies of the ^{2}H-labelled formate isotopic effect), and the enzyme operate via a ternary complex (FDH-formate-NAD^{+}) kinetic mechanism [107, 170–178].

4.3.2 The Metal-Dependent Formate Dehydrogenases

Several experimental and some computational approaches have been exploited to elucidate how the metal-dependent FDHs carry out the formate/CO_2 interconversion and over the years a few mechanistic proposals have been put forward [116, 117, 137, 166, 169, 179–185]. Presently, several key points are well established, but two remain a matter of debate, and all are discussed below, before the currently accepted mechanistic hypotheses are introduced.

(a) ***Presently, several key points are well established***

(i) The formate/CO_2 interconversion occurs at the molybdenum or tungsten centre, in a reaction that is intermediated by the metal, which cycles between the +6 and +4 oxidation states (Eq. 5a–5d), as demonstrated by numerous spectroscopic and kinetic studies. The electrons necessary to carry out CO_2 reduction or released from formate oxidation are intramolecularly transferred from the physiological partner (electron donor or electron acceptor), through the different redox centres of each enzyme (Fe/S centres, haems, FAD (see above)) that act like a "wire" to facilitate the fast and effective electron transfer. Therefore, the intramolecular electron transfer is, thus, an integral aspect of the global reaction. Depending on the enzyme (on the biochemical pathway where the enzyme is involved in), the physiological redox partner can be membrane

quinols, cytoplasmatic and periplasmatic cytochromes, ferredoxins, NAD(P) or coenzyme F_{420} [94–101]. For those enzymes like the dihydrogen-dependent CO_2 reductase (see above), the electrons are directly provided by the co-substrate oxidation (dihydrogen in this case) that occurs in the enzyme second active site. As a consequence of the physical separation of the oxidation and reduction half-reactions (that occur at different enzyme centres), all these enzymes operate via a ping-pong kinetic mechanism, as observed experimentally.

$$HCOO^- + Mo/W^{6+} \rightleftharpoons CO_2 + H^+ + Mo/W^{4+} \quad (5a)$$

$$Mo/W^{4+} + \text{Physiol. Partner}^{\text{oxidised}} \rightleftharpoons Mo/W^{6+} + \text{Physiol. Partner}^{\text{reduced}} \quad (5b)$$

$$CO_2 + H^+ + Mo/W^{4+} \rightleftharpoons HCOO^- + Mo/W^{6+} \quad (5c)$$

$$Mo/W^{6+} + \text{Physiol. Partner}^{\text{reduced}} \rightleftharpoons Mo/W^{4+} + \text{Physiol. Partner}^{\text{oxidised}} \quad (5d)$$

(ii) Although the formate/CO_2 interconversion occurs at the molybdenum or tungsten centre, the reaction is not one of oxygen atom transfer, as is characteristic of many molybdoenzymes and tungstoenzymes (Fig. 12) [94, 97, 110–112, 162–165]: the substrate for "CO_2 reduction" is in fact CO_2 and not hydrogencarbonate (Eq. 6) [186], and the product of formate oxidation is CO_2 and not hydrogencarbonate (Eq. 7), as was clearly demonstrated by the formation of $^{13}C^{16}O_2$ gas during the oxidation of ^{13}C-labelled formate in ^{18}O-enriched water [166]. Therefore, to catalyse the formate oxidation, FDH has to abstract one proton plus two electrons (Eq. 8) or one hydride (Eq. 9) from the formate molecule (or the reverse for CO_2 reduction).

$$HOCOO^- + 2e^- + 2H^+ \not\longrightarrow HCOO^- + H_2O \quad (6)$$

$$HCOO^- + H_2O \not\longrightarrow HOCOO^- + 2e^- + 2H^+ \quad (7)$$

$$HCOO^- \rightleftharpoons CO_2 + 2e^- + H^+ \quad (8)$$

$$HCOO^- \rightleftharpoons CO_2 + H^- \quad (9)$$

(iii) A simple chemical reasoning, based on the pK_a values of formic acid ($HCOOH/HCOO^-$ = 3.77; $HCOO^-/CO_2^{2-} \gg 14$), demonstrates that it is

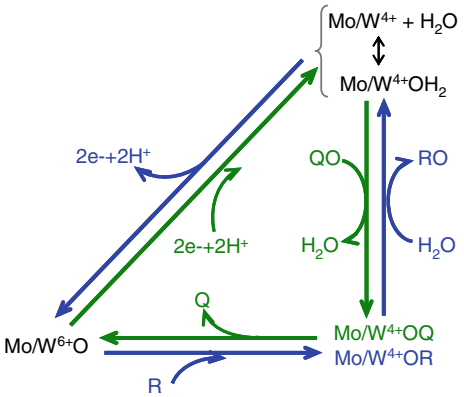

Fig. 12 Oxygen atom transfer in molybdo—and tungstoenzymes. Typically, these enzymes catalyse the transfer of an oxygen atom from water to product—oxygen atom insertion (blue arrows)—or from substrate to water—oxygen atom abstraction (green arrows)—in reactions that entail a net exchange of two electrons, in which the molybdenum/tungsten atom cycle between Mo/W^{6+} and Mo/W^{4+}, and, most importantly, where the metal is the direct oxygen atom acceptor or donor. This feature was coined by Holm and others in the 1980s as the "oxo transfer hypothesis"

much more difficult to abstract the Cα proton from formate (Eq. 8) than abstract a hydride (Eq. 9), which, in addition, lead to the formation of a stable product (CO_2), instead of a carbonanion (CO_2^{2-}) (Scheme 1). The simple mechanistic strategy followed by the metal-independent FDHs (Sect. 4.3.1.), that is, direct reaction with NAD^+, with no enzyme cofactors involved, further confirms that it must be exceptionally facile (thermodynamics) to abstract a hydride from the formate molecule. On its turn, CO_2, with an electronic structure $O\ {}^{-\delta}C^{+2\delta}\ O^{-\delta}$ and a carbon-localised LUMO, is susceptible to attack by nucleophiles and to reduction, being a good hydride acceptor, as supported by the chemistry of several synthetic transition metal-hydride complexes that mimic the FDH catalysis [65, 67, 187–192].

(iv) The terminal sulfido group of the active site (Fig. 10) is well documented as a hydride acceptor/donor. Since the 1970s, the sulfido group is established as the hydride acceptor in the oxidised molybdenum centre (Mo^{6+}=S) of xanthine oxidase and aldehyde oxidase[6] [110–112, 162–165, 193–202], as well

[6] Xanthine oxidase catalyses the hydroxylation of xanthine to urate. To carry out this reaction, xanthine oxidase promotes the cleavage of the C8–H bond of xanthine, with the hydride being transferred from the xanthine moiety to the active site sulfido group (Mo^{6+}=S → Mo^{4+}–SH); simultaneously, the active site catalyses the insertion of an oxygen atom in the xanthine moiety to produce urate (Mo^{6+}–O^- → Mo^{4+}). Aldehyde oxidase catalyses the conversion of aldehydes into the respective carboxylates, following the same chemical strategy: cleavage of the C–H bond, with transfer of hydride to the sulfido group, and subsequent insertion of an oxygen atom.

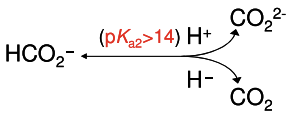

Scheme 1 Products formed by proton abstraction (ruled by a $pK_{a2} >> 14$) or hydride abstraction from formate

as, the hydride donor in the reduced centre (Mo^{4+}–SH) of hydroxybenzoyl-CoA reductase[7] [203, 204]. This "twin" behaviour (oxidised/hydride acceptor *versus* reduced/hydride donor) is supported by a remarkable characteristic of the Mo/W-ligands: the pK_a values of the coordinated ligands change dramatically with the oxidation state of the metal and determine that the higher oxidation states should hold deprotonated ligands, that is Mo/W^{6+}=S, while the lower oxidation states should hold protonated ligands, that is Mo/W^{4+}–SH [205–207]. This behaviour (Eq. 10) enables the metal-sulfido to act as a hydride acceptor/donor and is supported by the high covalency of the terminal sulfur atom in the metal sulfido group, with an available S π-bond well suited to accept a hydride.

$$Mo/W^{6+} = S + (2e^- + H^+) \rightleftharpoons Mo/W^{4+} - SH \tag{10}$$

The involvement of the sulfido group as the hydride acceptor during FDH catalysis was demonstrated by electron paramagnetic resonance (EPR) spectroscopic studies that showed that, in formate-reduced FDH, the formate Cα hydrogen atom is transferred to an acceptor group located within magnetic contact to the molybdenum atom of FDHs from different sources (*E. coli* [166], *D. desulfuricans* [136] or *Cupriavidus necator* (previously known as *Ralstonia eutropha*) [184]). The observation of a strongly coupled, solvent-exchangeable and substrate-derived proton, with a hyperfine constant of 20–30 MHz, is consistent with the hydrogen atom being transferred to a ligand in the first coordination sphere of the molybdenum atom upon its reduction [196, 197, 200, 201, 208]. Similar hyperfine constant values were determined in model complexes [209] and also in real enzymes, as in xanthine oxidase, where the strong coupled hydrogen is originated from the xanthine C8 hydrogen atom (the position that is hydroxylated by that enzyme (see Footnote 6) [196–198, 200–202, 208]. It should be noted that a hyperfine interaction of this magnitude could not arise from the transfer of the formate Cα hydrogen atom to an acceptor in the second coordination sphere of the metal, for example, transfer to the conserved histidine residue, as initially proposed [116, 117, 166, 169, 180–183], or transfer to the selenocysteine/cysteine residue if it had been dissociated from the

[7] Hydroxybenzoyl-CoA reductase catalyses the reverse reaction of the xanthine oxidase one, with insertion of a hydride and abstraction of an oxygen atom.

molybdenum/tungsten ion [117, 169, 180–183]—an hypothesis discussed below in point (vi). Photolysis assays with ^{77}Se-enriched FDH, described below in point (vi) and Footnote 8, further confirmed that the selenocysteine residue cannot be the hydrogen atom acceptor [166].

Further evidence that the sulfido group becomes protonated upon reduction was also provided by a recent X-ray absorption spectroscopy (XAS) study with the *R. capsulatus* Mo-FDH [210].

(v) The terminal sulfido group is essential to both formate oxidation and CO_2 reduction. It is well established, by numerous spectroscopic and kinetic studies, that cyanide reacts with the active site sulfido group of different molybdoenzymes, such as xanthine oxidase, and abstracts it in the form of thiocyanate, yielding a desulfo enzyme form that harbours an oxo group in the place of the native sulfido group [110–112, 193–195, 198, 199, 202]. The sulfido by oxo replacement renders xanthine oxidase and other enzymes inactive, because its active site is no longer able to accept a hydride (see Footnote 6). The same and complete cyanide inhibition is observed in several FDH, such as the ones from *Methanobacterium formicicum* [211], *Alcaligenes eutrophus* [212], *E. coli* [167], *R. capsulatus* (where the sulfido was observed to be replaced by an oxo group) [210], or *D. desulfuricans* (where thiocyanate formation accounted to 0.87 per molybdenum atom) [137]. Together with the experimental evidences that support the involvement of the sulfido group as a hydrogen atom acceptor during FDH catalysis (described above), these inhibitory results demonstrate that the sulfido group acts as a hydride acceptor/donor in FDH catalysis.

(b) ***Two interrelated points are not yet consensual***

(vi) Does the active site cysteine or selenocysteine residue dissociate from the metal during catalysis?

If the configuration of the oxidised active site is consensually accepted, the reduced form still finds a few contradictory experimental evidences (Fig. 10).

X-ray crystallography: In a reinterpretation of the crystallographic data of the reduced *E. coli* SeCys–Mo–FDH H originally obtained by Boyington et al. in 1997 [116], Raaijmakers and Romão in 2006 [117] suggested that the polypeptide loop containing the selenocysteine was not properly traced in the original work and that the selenocysteine residue is not bound to the metal, but, instead, is found dissociated from the molybdenum ion and shifted away (12 Å) (Fig. 4). Therefore, those authors suggested that, while in the oxidised state the selenocysteine residue is coordinated to the metal, the enzyme reduction triggers the residue dissociation, resulting in a square pyramidal penta-coordinated centre, where the molybdenum ion is coordinated by the *cis*-dithiolene (–S–C = C–S–) group of two pyranopterin cofactor molecules (in the equatorial positions) plus the terminal sulfido group (in the axial position) (Fig. 10). Regardless of this reinterpretation, all other

crystallographic structures so far available, for FDH and FMFDH (Figs. 4, 5, 6 and 9, and references herein), show a stable hexa-coordination, with the cysteine or selenocysteine always bound to the molybdenum/tungsten ion. This is also the case of the recently solved structure of the formate-reduced *D. vulgaris* SeCys–W–FDH [132] and also of the NADH-reduced *R. capsulatus* Cys–Mo–FDH, whose structure was determined by cryo-electron microscopy [139].

XAS: Two recent XAS studies at the Mo K-edge suggested that, in *R. capsulatus* Cys–Mo–FDH, the Mo^{5+} state holds the cysteine residue bound to the metal, as the oxidised Mo^{6+} one, with a Mo-S(Cys) bond of 2.63 Å, while the Mo^{4+} state of formate-reduced enzyme has its cysteine displaced form the metal [169, 210]. However, contrary results were obtained with SeCys–Mo–FDHs from *E. coli* [213] and *D. desulfuricans* [214], which showed a metal bound residue in all oxidised and reduced states: the *E. coli* enzyme EXAFS data at both the Mo and Se K-edges were interpreted as indicating the presence of one Mo–Se bond of 2.62 Å, plus one Se–S bond of 2.19 Å (between the sulfido group and the selenocysteine selenium) [213].

EPR spectroscopy: Further experimental evidence for the stable molybdenum/tungsten hexa-coordination came from EPR spectroscopy that clearly showed that the selenocysteine/cysteine must remain bound to the Mo^{5+} centre of formate-reduced enzyme [208]. When the EPR spectrum is obtained from ^{77}Se-enriched enzyme, a very strong and anisotropic interaction with selenium is observed ($A_{1,2,3}(^{77}Se)$ = 13.2, 75, 240 MHz) [166]. This interaction and the observation of the expected ^{95,97}Mo hyperfine coupling confirms that the selenium atom of the selenocysteine is directly coordinated to the Mo^{5+} and further suggests that the unpaired electron is delocalised over the selenium (17–27%) and molybdenum atoms (73–83%) [166]. Also, the hydrogen atoms of the β-methylene carbon of the selenocysteine residue are thought to be in the close proximity of the molybdenum atom, being responsible for an interaction with a not solvent-exchangeable protons (A_1 = 35.1 MHz) [136]. Photolysis assays additionally confirmed that the selenium/sulfur ligation is retained in the FDH Mo^{5+} centre (the light beam did not affect the strong selenium–molybdenum EPR interaction observed in ^{77}Se-enriched FDH)[8] [166]. The Mo^{5+} hexa-coordination (resulting from having the selenocysteine/cysteine residue bound to the molybdenum ion) was also supported by theoretical calculations on the signals-giving species of FDHs [215].

Inhibition assays: A different type of experimental evidence came from inhibition studies with iodoacetamide, an alkylating agent that reacts with "free" ionised selenocysteine or cysteine residues (carboxamidomethylation). Native *E. coli* SeCys–Mo–FDH H and its cysteine mutant [216] and native *R. capsulatus* Cys–Mo–FDH [183] are not inhibited by iodoacetamide treatment. However, when the preliminary iodoacetamide treatment (incubation) is carried out in the presence of formate (not under turnover), both native and cysteine-containing mutant *E. coli*

[8] These photolysis assays also demonstrate that the selenocysteine residue is not the formate Cα hydrogen acceptor [166]: while the light beam did not affect the ^{77}Se interaction, it induced the photolysis of the solvent-exchangeable formate-derived proton, showing that the selenocysteine residue does not bind the strongly coupled proton mentioned above.

FDHs are inhibited [216]. Inhibition is also observed in the *R. capsulatus* FDH, but only when the iodoacetamide treatment (incubation) is carried out in the presence of nitrate; in this case, the cysteine carboxamidomethylation was confirmed by mass spectroscopy [183]. On the other hand, native *D. vulgaris* SeCys–W–FDH is inhibited by iodoacetamide, but mass spectroscopy clearly showed that the inhibition is not due to the carboxamidomethylation of the active site selenocysteine residue (but of 9 other cysteine residues not present in the active site) [132]. In addition, other FDHs are not at all affected by iodoacetamide [135, 136]. Hence, the inhibition results available were not obtained under formate/CO_2 turnover conditions and the inconsistency of the results, once more, do not contribute to provide a definitive answer.

Overall, the majority of experimental evidences points towards a molybdenum/tungsten stable hexa-coordination, with the cysteine/selenocysteine residue always bound to the metal. Regarding the results showing a metal penta-coordination, with unbound cysteine/selenocysteine residue, it is possible that the crystallisation/irradiation had induced some artefacts that are not relevant to the enzyme activity; but it is also possible that the species crystallographically characterised, being catalytically relevant, bear no relation to the species observed by XAS and EPR (with these being not catalytically relevant). Certainly, high-resolution structures are needed to confirm the existence of the two alternating conformations of the selenocysteine/cysteine-containing polypeptide loop and to discuss the catalytic relevance of each conformation.

(vii) Do formate/CO_2 bind directly to the molybdenum/tungsten ion during catalysis?

Inspired by the oxotransfer chemistry displayed by several molybdenum—and tungsten-dependent enzymes (Fig. 12) [110–112, 162–165], and in particular by periplasmatic nitrate reductases[9], it was suggested that FDH catalysis necessarily involves the formate/CO_2 direct binding to the molybdenum/tungsten ion [180, 218].

To begin the discussion of this point, it should be noted that the direct formate/CO_2 binding would involve an unprecedented hepta-coordinated

[9] The *C. necator* periplasmatic nitrate reductase catalyses the reduction of nitrate to nitrite ($ONO_2^- + 2e^- + 2H^+ \rightarrow NO_2^- + H_2O$), and it was described to share with FDHs the same molybdenum coordination sphere, with the *cis*-dithiolene (–S–C = C–S–) group of two pyranopterin cofactor molecules, one terminal sulfido group and one sulfur atom from a cysteine residue [217]. The similarity in the active site metal centre led some authors to suggest similar mechanistic strategies for nitrate reductases and FDHs—leading to the so-called sulfur-shift mechanism [180, 218].

To give further support to the hypothesis of a similar mechanistic strategy, the nitrate reductase activity of different FDHs was investigated. The *R. capsulatus* Cys-Mo-FDH was described to be able to catalyse the nitrate reduction to nitrite, even though at an extremely low catalytic constant (k_{cat}(nitrate) = 0.21 min^{-1} [183] that compares very poorly with k_{cat}(formate) = 2124 min^{-1} and $k_{cat}(CO_2)$ = 89 min^{-1} [182]), and the catalysis was suggested by XAS to involve the dissociation of the cysteine residue from the molybdenum ion, with the subsequent nitrate binding [183]. However, other FDHs failed to reduce nitrate (such as the ones from *D. desulfuricans* [135, 136], *D. vulgaris* [132]).

molybdenum/tungsten centre or it would depend on the dissociation of the cysteine/selenocysteine residue from the metal, in order to create a vacant position (penta-coordinated centre) for substrate binding. While the hypothesis of the hepta-coordinated metal centre was (so far) never perused, the dissociation of the cysteine/selenocysteine is, as discussed above, controversial.

The two recent XAS studies mentioned above in point (vi) suggested that, in the presence of formate, the cysteine ligation of (active) *R. capsulatus* Cys–Mo–FDH is replaced by a long Mo–O bond of 2.15 Å, which was interpreted as arising from the Mo–OCO(H) complex [169, 210]. The strong and competitive inhibition of *E. coli* SeCys–Mo–FDH H-catalysed formate oxidation by azide, cyanate, thiocyanate, nitrite and nitrate (1–00 μM range) was also evoked to support that formate, as well as those inhibitors, bind directly to the molybdenum ion [219]. Yet, competitive inhibition can arise if the inhibitor binds in the active site, but not directly to the metal[10] [220]; this seems to be the case at least of azide, a well documented inhibitor of both metal-independent [104, 171, 177] and metal-dependent [136, 166] FDHs (as suggested by EPR [136, 215]) and nitrite (as suggested by crystallography[11]). Regarding nitrate, (once more) several other FDH enzymes are not inhibited or the inhibition constants are 2–3 orders of magnitude higher than K_m(formate) [132, 135, 136, 166], or it is though as a substrate (even though a very poor one; see Footnote 9 [182]). Moreover, the same study [219] showed that the inhibition of the *E. coli* SeCys-Mo-FDH H-catalysed CO_2 reduction by those anions is very weak (in the range of 1–50 mM) and not competitive in nature, results that are contradictory to the hypothesis that the reduced active site (the one that reacts with CO_2) becomes penta-coordinated, with an unbound selenocysteine residue, and with an available position to bind inhibitors and CO_2.

Therefore, except from the abovementioned XAS data, there are no other direct experimental evidences of the direct formate or CO_2 binding to the FDH molybdenum/tungsten ion; namely, there are no crystallographic structures showing the formate molecule in the active site and there are no EPR signals showing the presence of formate in the first coordination sphere of molybdenum/tungsten [136, 166, 184].

[10] The active site conserved arginine residue, below suggested to be key to "anchor" formate and CO_2 during turnover, could also be involved in the binding of these inhibitory anions through electrostatic interactions—to have a strong and competitive inhibition of the formate oxidation, it is not necessary that those anions bind directly to the molybdenum/tungsten ion it self.

The observed very weak inhibition of the CO_2 reduction by those anions (mentioned below in this point (vii)) could be explained by subtle conformational changes involving the conserved histidine residue upon reduction of the active site. Such conformational changes were described for *D. vulgaris* FDH [132] and could explain why those inhibitory anions would not be stabilised at the arginine spot within the reduced active site. Therefore, both the formate oxidation (strong inhibition) and the CO_2 reduction (weak inhibition) could be inhibited without evoking the direct binding of the inhibitory anions to the metal or the dissociation of the selenocysteine residue.

[11] Boyington et al. [116] described the structure of *E. coli* SeCys-Mo-FDH treated with the inhibitor nitrite as showing the selenocysteine bound to the molybdenum ion and the nitrite molecule with one of its oxygen atoms at 2.58Å from the molybdenum.

Theoretically, it can be argued that, since the FDH-catalysed reaction does not involve the transfer of an oxygen atom (as explained above in point (ii)), there is no need to form the otherwise expected Mo/W^{6+}–OCO(H) or Mo/W^{4+}–OCO complexes (follow Mo^{4+}–OR and Mo^{4+}–OQ in Fig. 12). It can also be argued in the opposite way: if formate/CO_2 binds directly to the molybdenum/tungsten ion, why there is no oxygen atom transfer to form hydrogencarbonate (Eq. 7)? Overall, in the absence of more definitive experimental evidences, we must continue to ask: Does the direct formate/CO_2 binding to the metal occur? Is it necessary or desirable to interconvert formate and CO_2? Is the penta-coordinated metal centre with unbound cysteine/selenocysteine catalytically relevant?

(c) ***Currently accepted mechanistic hypotheses***

In accordance with the well-established points (i) to (v) highlighted above, the FDH-catalysed formate oxidation and CO_2 reduction are presently recognised to occur through hydride transfer (Eq. 9), with the oxidised and reduced active site sulfido group, Mo/W^{6+}=S and Mo/W^{4+}–SH, acting as the direct hydride acceptor and donor, respectively. Yet, points (vi) and (vii) still raise questions to some authors regarding the coordination of the active site and substrates binding during FDH catalysis.

As originally proposed by Niks et al. [184] for formate oxidation and shortly after also for CO_2 reduction [137], we suggest that FDH catalysis proceeds as follows (the reaction mechanism is suggested to be identical in Mo–FDH and W–FDH, as well as in FMFDH):

Formate oxidation (Fig. 13, blue arrows) is initiated with the formate binding to the oxidised active site, but not directly to the molybdenum/tungsten atom. Following the example provided by the metal-independent FDH, where the formate-binding site harbours arginine and asparagine residues [102–109], it is suggested that the conserved arginine residue is essential to drive the formate Cα hydrogen towards the sulfido ligand, by establishing hydrogen bond(s) with its oxygen atom(s). Also, azide (N_3^-, isoelectronic with CO_2) is suggested to bind (tightly) to the same site and not directly to the molybdenum/tungsten ion (as had been previously suggested for the *D. desulfuricans* FDH inhibition by azide [136, 215]). The binding of azide and formate to the same site, and not to the molybdenum/tungsten atom itself, explains why azide is a powerful inhibitor of both metal-independent (K_i = 40 nM for *Candida boidinii*) [104, 171, 177] and metal-dependent FDHs [136, 166]. A similar reasoning applies to the inhibitor nitrite (isoelectronic with formate). Formate oxidation, then, proceeds by a straightforward hydride transfer from formate to the sulfido group of the oxidised molybdenum/tungsten centre, Mo/W^{6+}=S, leading to the formation of Mo/W^{4+}–SH and CO_2. The re-oxidation of Mo/W^{4+} to Mo/W^{6+} (via intramolecular electron transfer to the enzyme other(s) redox centre(s) and, eventually, to the physiological partner) and the release of CO_2 close the catalytic cycle. The now oxidised Mo/W^{6+} favours the sulfido group deprotonation (dictated by the ligand pK_a [205–207]), and the initial oxidised

molybdenum/tungsten centre, Mo/W^{6+}=S, is regenerated. Under non-steady-state catalytic conditions (as the ones created in EPR experiments) the molybdenum/tungsten one-electron oxidation should be favoured ($Mo/W^{4+} \rightarrow Mo/W^{5+}$), leading to the formation of the EPR detectable Mo^{5+}–SH species.

CO_2 reduction is suggested to follow the reverse reaction mechanism (Fig. 13, green arrows). First, CO_2 binds to the reduced active site, not directly to the molybdenum/tungsten ion, but at the same site as formate (and azide), with the conserved arginine anchoring its oxygen atom(s) through hydrogen bond(s) and orienting its carbon atom towards the protonated sulfido ligand. In an approximated way, based on the inhibition and Michaelis–Menten constants for the *D. desulfuricans* FDH, the "binding strength" is suggested to follow the order CO_2 ($K_m \approx 15$ μM [137]) > azide ($K_i \approx 30$ μM [136]) > formate ($K_m \approx 60$ μM [137]). Then, the reaction proceeds through straightforward hydride transfer from the protonated sulfido group of the reduced molybdenum/tungsten centre, Mo/W^{4+}–SH, to the CO_2 carbon, whose LUMO have predominant C–π orbital character, prone to nucleophile attack and reduction. This yields a formate moiety and Mo/W^{6+}=S. The subsequent re-reduction of Mo/W^{6+} to Mo/W^{4+} (via intramolecular electron transfer from the enzyme physiological partner, through its redox centre(s)) and formate release closes the catalytic cycle. The now reduced Mo/W^{4+} favours the sulfido group protonation and the initial reduced molybdenum/tungsten centre, Mo/W^{4+}–SH, is regenerated.

The FDH-catalysed reaction is reversible and the equilibrium between formate oxidation *versus* CO_2 reduction is determined by the availability of formate *versus* CO_2 and the ability to maintain the active site oxidised (Mo/W^{6+}) *versus* reduced (Mo/W^{4+}), which, in its turn, determines the protonation state of the metal sulfido group in a concerted and straightforward way.

Overall, the chemical strategy herein suggested is exactly the same as the one proposed for the metal-independent FDHs: both bind formate in a close proximity to an oxidised, electrophilic, hydride acceptor, which in metal-independent enzymes is a NAD^+ molecule and in metal-dependent enzymes is the M^{6+}=S group; both bind CO_2 in a close proximity of a reduced, nucleophilic, hydride donor, a NADH molecule or the M^{4+}–SH group.

As expected, this mechanistic proposal faces some criticism and the most relevant one concerns the role of the active site selenocysteine/cysteine residue. In fact, although the mechanism is suggested to operate in a hexa-coordinated metal centre (Fig. 13), it can also take place in a penta-coordinated centre (Fig. 10), with an unbound selenocysteine/cysteine—the sixth ligand does not seem to interfere with the hydride transfer[12]. Even though there are experimental evidences (as discussed above) and mechanistic arguments can be envisaged to support the necessity of having a bound selenocysteine/cysteine (as discussed in [96, 98]), in the absence of

[12] It should be noted that, xanthine oxidase, for example, that also uses a terminal sulfido group as the hydride acceptor in the conversion of xanthine to urate, has a molybdenum penta-coordinated active site, with no amino acid residues bound to it (the molybdenum ion is coordinated by the *cis*-dithiolene (–S–C = C–S–) group of one pyranopterin cofactor molecule, the terminal sulfido group plus two oxo groups (see previous Footnotes and references in the text).

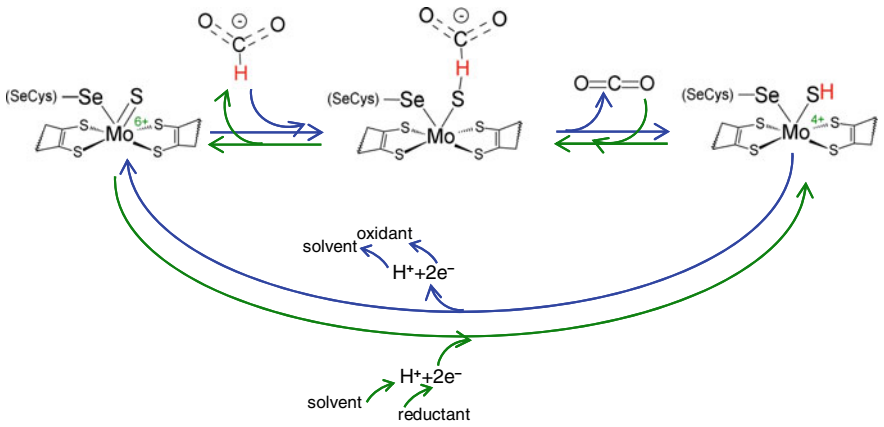

Fig. 13 Reversible hydride transfer mechanism proposed for metal-dependent formate dehydrogenase and *N*-formyl-methanofuran dehydrogenase [137, 184]. Reaction mechanism proposed for formate oxidation (blue arrows) and CO_2 reduction (green arrows). For simplicity, the mechanism is represented only for a molybdenum, selenocysteine-containing enzyme, but it should be similar for tungsten and cysteine-containing enzymes. See text for details. A similar hydride transfer mechanism can also take place with a penta-coordinated reduced metal centre, with a dissociated selenocysteine/cysteine residue (see text for details)

clear and definitive experimental evidences, both scenarios—*dissociated and bound selenocysteine/cysteine*—seem to be possible and this is an aspect that will remain in open for now. Certainly, future research will shed light in these aspects of the FDH reaction, allowing a critic evaluation of this mechanistic proposal.

4.4 Formate Dehydrogenases in the Context of Carbon Dioxide Utilisation

The majority of currently known FDHs function in vivo to oxidise formate, with only a few participating in metabolic pathways to reduce (fix) CO_2—the reaction direction that is interesting to "solve humankind's problem" with atmospheric CO_2. However, the CO_2/formate interconversion is thermodynamically reversible ($E^{\circ\prime}$ (CO_2/$HCOO^-$) = −0.43 V) and in vitro there is no a priori reason for a FDH to be unable to catalyse the CO_2 reduction, as long as there is sufficient reducing power available[13]. Regarding the metal-independent FDHs, this simply means the adequate NADH/NAD^+ ratio (Eq. 11); in what concerns the metal-dependent FDHs,

[13] *In vivo*, in the great majority of the cases, the reaction is tuned to operate only in one direction; this is determined by the reduction potential of the enzyme redox centres, by the available physiological electron partners and substrates and by the redox status of the subcellular location where the reaction takes place. The few exceptions are mainly related with regulation points of the metabolism.

this means that the molybdenum/tungsten active site centre must be kept reduced at the proper reduction potential (Eq. 12). Although at first sight obvious, the necessity to keep the enzyme active site reduced is most often overlooked, what may explain why there are so many reports in the literature of FDHs unable to reduce CO_2. This is particularly true for metal-dependent FDHs: if the reduction potential of one (or more) of the FDH redox centres is (are) relatively high, it could be difficult to "push" the electrons into the active site (the centre with the higher reduction potential could stay reduced, "blocking" the electron transfer to the other (s) centre(s) with lower reduction potentials and the active site in particular). In addition to thermodynamics, also the kinetics has to be taken into account to evaluate if the CO_2 reduction is going to be efficient, or too slow relatively to the formate oxidation to be relevant (rate of formate oxidation versus CO_2 reduction, Eqs. 13, 14). The key point here is that FDH kinetics is determined by four parameters, the K_m and k_{cat} for the two substrates (CO_2 and formate), and the reaction can be run under different regimes (mainly forward, mainly reverse and equilibrium, as determined by k_{cat}/K_m and imposed conditions). However, except for protein engineering (a difficult task on its own), there is not much that can be done to modify the kinetic parameters to further favour the CO_2 reduction.

$$CO_2 + NADH \rightarrow HCOO^- + NAD^+ \tag{11}$$

$$CO_2 + FDH\left(Mo/W^{4+}\right) \rightarrow HCOO^- + FDH\left(Mo/W^{6+}\right) \tag{12}$$

$$CO_2 + A_{red} \overset{k^{CO_2}}{\rightarrow} HCOO^- + A_{ox} \tag{13}$$

$$HCOO^- + A_{ox} \overset{k^{HCCO-}}{\rightarrow} CO_2 + A_{red} \tag{14}$$

Also, the enzymes stability and potential interfering compounds must be well thoughtout. The lifetime of a CO_2 converter device is a critical issue, and it would greatly depend on the time the enzyme maintains its full activity. In this respect, it should be emphasised that the purifying processes often decrease the enzymes stability and even make them unstable (while taken out of their biological environment), thus hampering their usage in a sustained ("real life") way or just making the scale up process unviable. The inhibition and inactivation by compounds that might be present in the "substrate reaction mixture"; for example, dioxygen or carbon monoxide, are pitfalls that must be considered to avoid the need (additional cost) of using purified CO_2. The inhibition or inactivation (or, on the contrary, improved stability) by the materials used to build the device cannot be overlook also.

The enzyme–material "communication" is another major challenge in hybrid systems. It is necessary to properly orient and "link" the enzyme to the material (for example, electrode or light absorber), via electrostatic or covalent interactions to maximise the charge transfer. In this respect, features as the enzyme size (in the

nanoscale) and local-specific surface charge/hydrophilicity/hydrophobicity must be taken into consideration when choosing the materials and its functionalisations.

Having these general points tackled, any FDH could be used to build a device to promote the CO_2 reduction. The same would be true for whole-cell devices, but considering in that case the organism whole metabolism (carbon and energy needs).

4.5 Formate Dehydrogenases in Action

The use of enzymes and whole-cells systems to convert CO_2 into VC is growing exponentially due to the "green" advantages the "biochemical way" can offer, namely substrate and product specificity (ability to discriminate the substrate in a complex mixture and to produce only the product of interest) in reactions at ambient temperature and pressure and neutral pH. Numerous hybrid systems are currently being exploited to convert CO_2 into formate, following the same master lines as described in Sect. 3 (Fig. 2). Like electrochemistry, bioelectrochemistry is currently under intense research, as is reviewed in [221–227] and references herein (below). Most interest is also being focused on the biophotoreduction of CO_2, as solar light represents the most straightforward way to use a RES to convert CO_2. Semi-artificial photosynthesis systems have been devised, where enzymes and also entire metabolic pathways within cells are interfaced with synthetic materials to develop new solar-to-VC and solar-to-fuel devices, which would not be feasible with natural or artificial systems alone [228 and references herein (below)]. The direct CO_2 hydrogenation is also getting enormous attention, mimicking metabolic pathways, where the formate-hydrogen lyase systems are the most explored examples, but using also whole-cells systems. Most important are the breakthroughs achieved by exploiting the recently identified metabolic pathways of acetogens and its dihydrogen-dependent CO_2 reductase enzymes (Sect. 4.2.2.), as is reviewed by Litty and Müller in this Book [152] and also [153–159] and references herein (below).

Herein (below), a few promising studies and successful proof of concepts of FDH-dependent CO_2 reduction to formate and beyond are discussed, to highlight the power of FDHs and the challenges this CO_2 bioconversion still faces.

One of the most efficient CO_2 reducers so far described (along with the *T. kivui* enzyme described below) is a SeCys–W–FDH from the *Synthrobacter fumaroxidans* that displays an impressive rate of CO_2 reduction of $\approx 2.5 \times 10^3 s^{-1}$ (reported as $900 U mg^{-1}$; K_m^{CO2} not determined, assays with 10 mM hydrogencarbonate), with a slightly lower formate oxidation rate ($\approx 1.9 \times 10^3 s^{-1}$ (reported as $700 U mg^{-1}$); $K_m^{HCOO^-}$ of 40 μM) [229–231]. This enzyme is also a good electrocatalyst to carry out the electrochemical reduction of CO_2 to formate, using mild conditions and applying small overpotentials, with a maximum current density of $\approx 80\ \mu A cm^{-2}$ that corresponds to $\approx 110\ s^{-1}$ (from a monolayer of enzyme) [232]. Intriguingly, while in homogeneous catalysis in solution the CO_2 reduction is slightly faster than the formate oxidation, in the electrochemical-assisted reduction/oxidation is the formate oxidation that is more than 2 times

faster (with a current density of $\approx$ 200 μAcm^{-2} [232]). *S. fumaroxidans* expresses another very fast CO_2 reducer SeCys-W-FDH, with a rate of $\approx$ 200 s^{-1} (reported as 90Umg^{-1}) [229–231], but its CO_2 reduction activity cannot kinetically compete with its highly efficient formate oxidation, rate of $\approx 5.6 \times 10^3 s^{-1}$ (value reported as 2700Umg^{-1}) and $K_m^{HCOO^-}$ of 10 μM. Unfortunately, these enzymes are extremely oxygen-sensitive, and no further studies towards a biotechnological application were pursuit, as far as we know.

Several other FDHs have been described to be able to reduce CO_2, but at considerably lower rates. Numerous studies have been conducted with metal-independent FDHs, many of which relying on sacrificial electron donors [233–248]. This is the case of the *C. boidinii* NAD-dependent metal-independent FDH, that, in spite of its considerably low $k_{cat}^{HCO3^-}$ value of only 0.009 s^{-1} ($K_m^{HCO3^-} \approx$ 27.3 mM [240]; $k^{HCO3^-} \approx 0.3\ M^{-1}s^{-1}$; $k_{cat}^{HCOO^-} \approx 5.0\ s^{-1}$; $K_m^{HCOO^-} \approx 5.0$ mM; $k^{HCOO^-} \approx 1.0 \times 10^3 M^{-1}s^{-1}$ [109]), has been largely exploited for its ability to reduce CO_2. To push the reaction in the desired, but thermodynamically unfavourable, direction[14] is important to remove NAD^+/regenerate NADH (also essential for the process to become cost-effective, since NADH is a very expensive reducing agent). Four selected examples of different strategies to force the reaction towards the CO_2 reduction are: (a) an electroenzymatic cell where NADH is electrochemically regenerated through a rhodium complex, with which a formate formation rate of $\approx 3.2 \times 10^{-4}$ μmolmin^{-1}mg^{-1} was achieved [240]; (b) electrochemical NADH regeneration, but with an electropolymerised mediator-regenerator (neutral red) in a novel cathode with immobilised FDH, which is able to produce formate at a rate of $\approx$ 60 μMmin^{-1}) [249]; (c) photocatalytical NADH regeneration using a rhodium complex and a visible light-active photocatalyst) that enabled a formate formation rate of $\approx$ 1 μmolmin^{-1} [250]; (d) and enzymatic regeneration, using glutamate dehydrogenase with NAD(H) being covalently attached to micro-particles, to be easily recovered and reused, in an approach that allowed to improve the reaction yield from 0.12 to 1.27 methanol formed/NADH consumed (in this study, formate was further reduced to methanol) [251]. The *Thiobacillus* sp KNK65MA NAD-dependent metal-independent FDH exhibit an as well low k_{cat} value ($k_{cat}^{HCO3^-} \approx 0.32\ s^{-1}$; $K_m^{HCO3^-} \approx 9.2$ mM; $k^{HCO3^-} \approx 35\ M^{-1}s^{-1}$), but its specificity for formate is only 3 times superior ($k_{cat}^{HCOO^-} \approx 1.8\ s^{-1}$; $K_m^{HCOO^-} \approx 16$ mM; $k^{HCOO^-} \approx 110\ M^{-1}s^{-1}$) [252]. This *Thiobacillus* enzyme was successfully used to reduce CO_2 by coupling it with a NADH photoelectrochemical regeneration system (Fig. 14), with a formate production rate of 2 μMmin^{-1} (current density $\approx$ 3.5mAcm^{-2}) [245].

The metal-dependent FDHs display a wide range of CO_2 reduction rates. The *Clostridium carboxidivorans* NAD-dependent SeCys-W-FDH exhibits a considerably low $k_{cat\,2}^{CO}$ value (only 0.08 s^{-1}; $K_m^{HCO3^-} \approx 50$ μM) [144, 145, 147].

[14] The reduction potential values of the $NAD(P)^+$/NAD(P)H (−0.32 V) and CO_2/$HCOO^-$ (−0.43 V) pairs indicate that the NADH-dependent CO_2 reduction (Eq. 11) is thermodynamically highly unfavourable. To force the reaction towards the CO_2 reduction is important to remove the product (NAD^+) and maintain (regenerate) the substrate (NADH) concentration.

Nevertheless, it enabled the photoelectrochemical CO_2 reduction to formate within an enzyme cascade that led to the methanol production at $\approx$ 4 μMmin^{-1}) [253]. The *Methylobacterium extorquens* AM1 NAD-dependent Cys-W-FDH has also been exploited with different approaches to drive the electrochemical CO_2 reduction [242, 254–258]. Using mediated enzymatic bioelectrocatalysis with gas diffusion electrodes[15], current densities of 15–20mAcm^{-2} were attained [254, 255]; in a whole-cell catalyst, *M. extorquens* was able to electrochemically produced formate concentrations of up to 60 mM [242].

The *R. capsulatus* [182] and *Cupriavidus oxalaticus* [259] NAD-dependent Cys–Mo–FDH enzymes, on the other hand, have $k_{cat\,2}^{CO}$ values, of 1.5 s^{-1} and $\approx$ 3 s^{-1}, respectively, but $\approx$ 25 and $\approx$ 30 times (respectively) lower than the one for formate oxidation (*R. capsulatus* $K_m^{HCOO-} \approx 280$ μM and $K_{m\,2}^{CO}$ not determined, assays with 100 mM hydrogencarbonate; *C. oxalaticus* $K_m^{HCOO-} \approx 100$ μM and $K_m^{HCO3-} \approx 40$ mM). The *C. necator* NAD-dependent Cys–Mo–FDH, on the contrary, catalyses the reduction of CO_2 with a $k_{cat\,2}^{CO} \approx 11$ s^{-1} ($K_{m\,2}^{CO} \approx 2.7$ mM; $K_m^{NADH} \approx 45$ μM) [260, 261]. To fulfil the potential industry application of this oxygen-tolerant and robust enzyme, it is necessary to implement a NADH regenerating system that pushes the reaction towards CO_2 reduction (as discussed above; see Footnote 14) [262]. With the *C. necator* FDH, this was successfully achieved with the inclusion of glucose dehydrogenase in the system (Fig. 15), which, while catalysing the re-reduction of NAD^+ to NADH, enabled the continuous electron delivery to drive the CO_2 reduction and, therefore, improved the reaction yield from 0.2 to 1.8 formate formed/NADH consumed [262].

The *E. coli* SeCys-Mo-FDH H was also shown to be able to reduce CO_2 [263], but at rates considerably lower than the ones of formate oxidation, < 1 *versus* 160 s^{-1} [263]. Interestingly, when the reaction is driven electrochemically (protein film voltammetry), the formate oxidation was only two times higher than the CO_2 reduction, with current densities of 180 *versus* 80 μAcm^{-2}, respectively [263]. This *E. coli* enzyme feature has been exploited in fuel cell devices (FDH immobilised in redox mediators-functionalised redox polymers) [15, 16], where CO_2 could be reduced with a very high Faradaic efficiency (99%) and a current density of $\approx$ 60 μAcm^{-2} ($K_m^{HCO3-} \approx 2.5$ mM) [16]. Thanks to the FDH H-containing formate-hydrogen lyase system (Sect. 4.2.2.)[16], engineered *E. coli* whole cells were also used as a "cell factory" to very efficiently produce formate from a gaseous mixture of CO_2 and dihydrogen (56:44; up to 10 bar) (Fig. 16); an 100% of CO_2 conversion was achieved, with formate (more than 500 mM) being accumulated outside the bacterial cells [264]. Intact *E. coli* cells were also used in a microbial

[15] Gas diffusion electrodes (GDE) promote electrochemical reactions between the liquid and the gaseous phase, thus eliminating the limitations arising from slow mass transport when hydrogencarbonate/carbonate is used as CO_2 source.

[16] Under physiological conditions the *E. coli* formate-hydrogen lyase system catalyses the formate oxidation to CO_2 coupled to the reduction of protons to dihydrogen (Sect. 4.2.2.); yet, under a pressurised (up to 10 bar) atmosphere of CO_2 and dihydrogen, engineered *E. coli* (with abolished "respiratory" FDH, pyruvate-formate lyase and all major hydrogenases) whole cells efficiently catalyse the reverse reaction of formate formation.

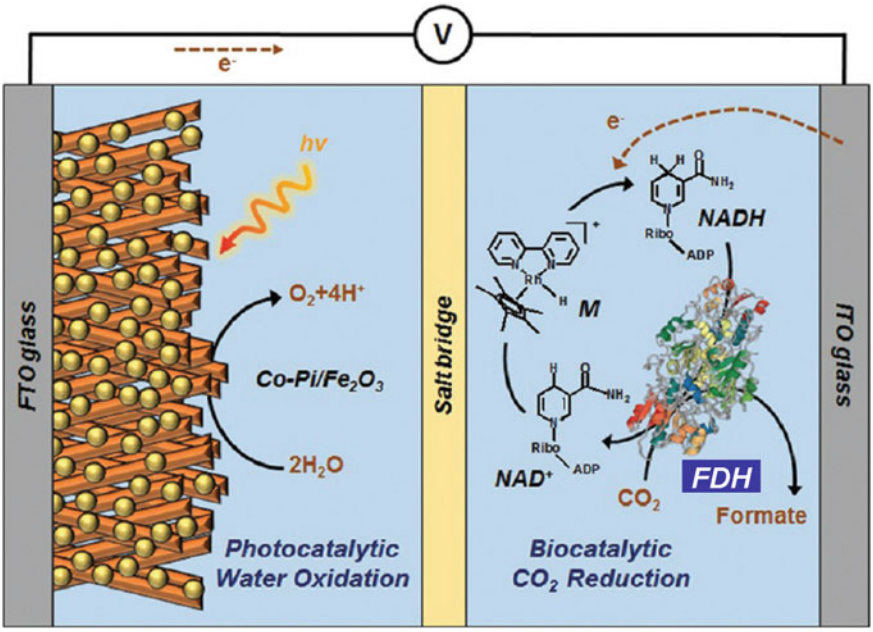

Fig. 14 Schematic diagram of enzymatic photosynthesis of formic acid using *Thiobacillus* FDH coupled with photoelectrochemical regeneration of nicotinamide cofactors. Co-Pi, cobalt phosphate. See text and Ref. [245] for details. Reproduced (from Ref. [245]) by permission of the Royal Society of Chemistry. All rights reserved. https://doi.org/10.1039/c6gc02110g

electrolysis system using an iron-modified carbon cathode, with which a formate production rate of $\approx 10\ \mu\text{Mmin}^{-1}$, with a Faradaic efficiency of $\approx 60\%$, was attained [265].

FDHs from sulfate-reducing bacteria constitute other very interesting systems to exploit, exhibiting high rates of CO_2 reduction. The *D. desulfuricans* SeCys–Mo–FDH is a strikingly efficient CO_2 reducer. With a $k_{cat}^{CO_2} \approx 50\ s^{-1}$ and particularly low $K_m^{CO_2} \approx 15\ \mu M$, this enzyme has a superior specificity for CO_2 ($k^{CO_2} \approx 3.3 \times 10^6 M^{-1}s^{-1}$) [137]. The high K_m value for formate ($K_m^{HCOO^-} \approx 55\ \mu M$; $k_{cat}^{HCOO^-} \approx 550\ s^{-1}$; $k^{HCOO^-} \approx 10 \times 10^6 M^{-1}s^{-1}$) enables *D. desulfuricans* SeCys–Mo–FDH to be a powerful CO_2 reducer, as long as the formate concentration is kept low (is removed from the system). In addition, once the catalysis is initiated (occurring at steady-state rates), this enzyme robustness allows the reaction to fully proceed even in the presence of dioxygen [139]. Moreover, the *D. desulfuricans* SeCys–Mo–FDH is also a good electrocatalyst (unmediated electrochemistry) to carry out the electrochemical reduction of CO_2 with good catalytic currents being attained [266]. The ability of *D. desulfuricans* to produce formate was also demonstrated in whole-cells catalysis, where the continuous formate production exhibited a maximum specific formate production rate of 14 mM formate/g_{dcw}h, and more than 45 mM of formate were obtained with a production rate of 0.40mMh^{-1} [267].

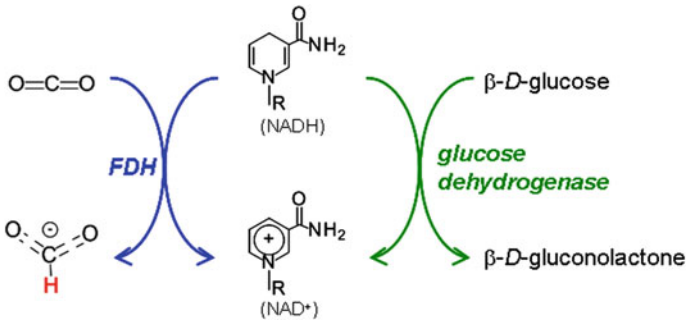

Fig. 15 Schematic diagram of the enzymatic cascade reaction *C. necator* FDH and glucose dehydrogenase. See text and Ref. [262] for details

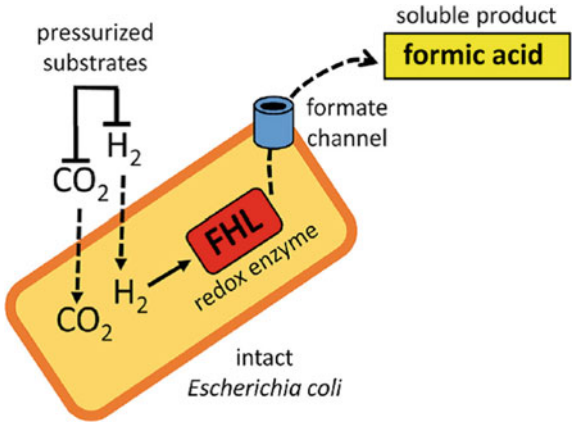

Fig. 16 Schematic diagram of a "cell factory" to produce formate using *E. coli* whole-cells. FHL, formate-hydrogen lyase. See text and Ref. [264] for details Adapted with permission from Ref. [264]. http://creativecommons.org/licenses/by/4.0/

The *D. vulgaris* contains also several interesting FDHs. One SeCys–Mo–FDH is able to catalyse the CO_2 reduction at a rate of $\approx$ 3.4 s^{-1} (reported as 1Umg^{-1}) [129, 131, 268]. However, its extremely low K_m value for formate ($K_m^{HCOO^-}$ of 8 μM) and higher rate of formate oxidation ($k_{cat}^{HCOO^-} \approx 260\ s^{-1}$) makes this enzyme a very interesting biocatalyst to oxidise formate instead, namely to be coupled to dihydrogen production. The proof of concept that *D. vulgaris* is able to produce dihydrogen at high volumetric and specific rates (0.125 dm^3 H_2/dm^3h^1 and 2.5 dm^3 $H_2/g_{dcw}h$) was obtained recently, with the demonstration that whole cells are able to grow by catalysing the oxidation of formate to hydrogencarbonate and dihydrogen, in the absence of sulfate or a syntrophic partner [268, 269].

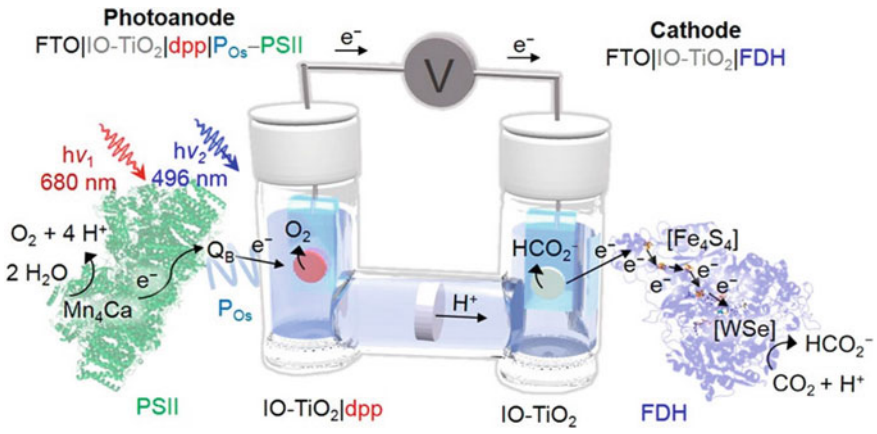

Fig. 17 Schematic diagram of a semi-artificial photosynthetic tandem PEC cell coupling water oxidation to CO_2 reduction by *D. vulgaris* FDH. dpp, phosphonated diketopyrrolopyrrole dye, P_{Os}, [poly(1-vinylimidazole-coallylamine)-[Os(bipy)$_2$Cl]Cl redox polymer], PS II, photosystem II. See text and Ref. [270] for details Adapted with permission from Ref. [270]

The *D. vulgaris* SeCys–W–FDH, on the other hand, is better suited for CO_2 reduction, with a $k_{\text{cat}\,2}^{\text{CO}} \approx 315\ \text{s}^{-1}$ ($K_m^{\text{CO}_2} \approx 420\ \mu\text{M}$; $k^{\text{CO}_2} \approx 0.75 \times 10^6\text{M}^{-1}\text{s}^{-1}$) [132]. Even though the CO_2 specificity of this enzyme is considerably lower (100 times) than that for formate ($k_{\text{cat}}^{\text{HCOO}^-} \approx 1310\ \text{s}^{-1}$; $K_{\text{m}}^{\text{HCOO}^-} \approx 17\ \mu\text{M}$; $k^{\text{HCOO}^-} \approx 77.5 \times 10^6\text{M}^{-1}\text{s}^{-1}$ [132]), this *D. vulgaris* W-FDH is at the base of several very well succeeded proof-of-principle devices for semi-artificial photosynthesis and production/storage of dihydrogen. A *D. vulgaris* W-FDH-containing cathode wired to a *T. elongatus* photosystem II-containing photoanode with a synthetic dye with complementary light absorption was successfully employed to drive light-dependent CO_2 conversion to formate, using water as an electron donor (Fig. 17) [270]. In this photoelectrochemical tandem device, electrons are photo-generated in the photosystem II, which oxidises water to dioxygen, and transferred to the FDH cathode (this biocathode catalyses the formate formation with a current density of 240 μAcm^{-2} (at—0.6 V versus SHE) and a Faradaic efficiency of 80%). The whole system is able to efficiently produce formate at 0.185 μmolcm^{-2}, with Faradaic efficiency of $\approx$ 70%, but progressive photosystem II photodegradation (due to prolonged irradiation) resulted in an irreversible decrease in the CO_2 photoreduction. A different *D. vulgaris* W-FDH-material configuration was recently devised, based on a ruthenium dye [271]. The employment of this dye-sensitised TiO_2-adsorped FDH enable the visible light-driven CO_2 reduction to formate with a turnover frequency of 11 s^{-1}, in the absence of a soluble redox mediator (Fig. 18) [271] (comparatively, this bioelectrode reached a current density of 100 μAcm^{-2} (at −0.6 V versus SHE), with a Faradaic efficiency of 92.5%). Furthermore, the *D. vulgaris* FDH-mediated electroenzymatic CO_2 reduction to formate was attained using a redox viologen-based polymer/enzyme-modified gas diffusion electrode

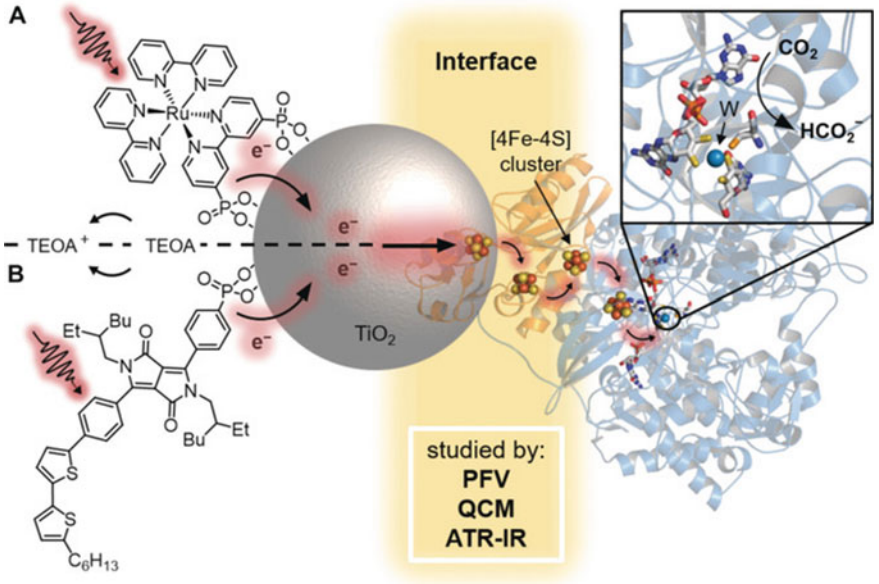

Fig. 18 Schematic diagram of a photocatalyst system for CO_2 conversion using a dye-semiconductor-*D. vulgaris* FDH arrangement. ATR-IR, attenuated total reflection infrared, PFV, protein film voltammetry, QCM, quartz crystal microbalance, TEOA, triethanolamine. See text and Ref. [271] for details Adapted with permission from Ref. [271]

[272]. The *D. vulgaris* W-FDH has also been exploited to drive the dihydrogen formation/storage in a system that mimics the natural formate-hydrogen lyase systems (see Sect. 4.2.2.) [273]. The semi-artificial formate-hydrogen lyase system consists of the *D. vulgaris* W-FDH and *D. vulgaris* Ni/Fe-Hase immobilised on a conductive scaffold of indium tin oxide that acts as an electron relay. This configuration enables the overall reaction to proceed reversibly towards formate conversion into CO_2 plus dihydrogen or towards formate formation, with minimal bias in either direction (Fig. 19), thus allowing the longed-for dihydrogen storage and release on demand. The system is able to produce dihydrogen (upon formate addition) at a rate of 4nmolmin^{-1} (turnover number of 23 $\times$ 10^3 and turnover frequency of 6.4 s^{-1} for the Hase) or to produce formate (in the presence of dihydrogen) at a rate of 22nmolmin^{-1} (turnover number of 16 $\times$ 10^3 and turnover frequency of e.4 s^{-1} for the FDH) for 8 h (this bioelectrode system reached current densities of 185 and 450 μAcm^{-2}, for CO_2 and H^+ reduction, respectively (at −0.6 V versus SHE) and of 300 and 440 μAcm^{-2} for formate and H_2 oxidation, respectively (at −0.2 V versus SHE), with Faradaic efficiencies for H_2 and formate production of 77 and 76%, respectively). Moreover, this semi-artificial formate-hydrogen lyase concept can be deployed in either an electrochemical cell or a self-assembled colloidal suspension, thus providing versatility for applications in different contexts.

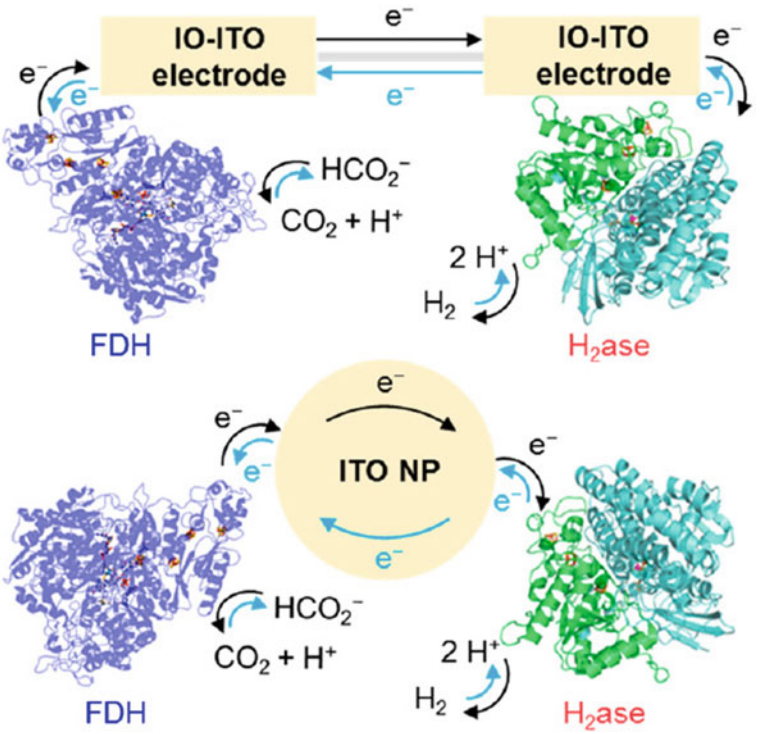

Fig. 19 Schematic diagram of a semi-artificial formate-hydrogen lyase system for the reversible and selective interconversion of dihydrogen and CO_2 into formate using *D. vulgaris* FDH. The concept can be deployed in either an electrochemical cell (top) or a self-assembled colloidal suspension (bottom). H_{2ase}, hydrogenase, ITO. indium tin oxide, NP, nanoparticle. See text and Ref. [273] for details Adapted with permission from Ref. [273]

Acetogens and methanogens are organisms that reduce (fix) CO_2 in vivo [274, 275], and, as such, they have been the focus of intense research to develop new CO_2 converter devices, enzymatic and whole-cell systems, as is reviewed by Litty and Müller in this Book [152] and also [153–159]. Herein, we only highlight the dihydrogen-dependent CO_2 reductases (Sect. 4.2.2.) from *Acetobacterium woodii* and *T. kivui*: the former is a SeCys–Mo–FDH that catalyses the CO_2 hydrogenation with a k_{cat} of 28 s^{-1} (reported as 10Umg^{-1}; $K_m^{HCO3-} \approx 37$ mM) and displays slightly higher rates of formate oxidation (CO_2 plus dihydrogen formation with a $k_{cat} \approx 39$ s^{-1}, reported as 14Umg^{-1}; $K_m^{HCOO-} \approx 1$ mM) [153, 154]; the second is a outstanding Cys–W–FDH that catalyses the CO_2 hydrogenation with a k_{cat} of 2.5 $\times$ $10^3 s^{-1}$ (900 µmol formate min^{-1}mg^{-1}; $K_m^{H2} \approx 130$ μM—one of the fastest CO_2 reducers so far described), with the reverse reaction being catalysed with a k_{cat} of 2.7 $\times$ $10^3 s^{-1}$ (930 µmol dihydrogen min^{-1}mg^{-1}; $K_m^{HCOO-} \approx 550$ μM) [156]. The CO_2 hydrogenation equilibrium constant close to one ($\Delta G^{o\prime}$ = 3.5KJmol^{-1}) makes these systems ideal biocatalysts for dihydrogen storage and production. *A. woodii*

was successfully used as a whole-cell biocatalyst to produce dihydrogen from formate, reaching a specific dihydrogen formation rate of ≈ 70 mmol $g^{-1}_{protein}1h^{-1}$ (≈ 30 mmol $g^{-1}_{cdw}h^{-1}$) and a volumetric dihydrogen evolution rate of ≈ 80 mMh^{-1}, with yields up to 1 mol dihydrogen per mol formate [155]. *T. kivui* was successfully exploited in a whole-cell system to convert dihydrogen plus CO_2 (hydrogencarbonate) into formate, achieving a specific formate formation rate of ≈ 235 mmol $g^{-1}_{protein}1h^{-1}$ (≈ 150 mmol $g^{-1}_{cdw}h^{-1}$) and a volumetric formate production rate of $270mMh^{-1}$; high titres up to 130 mM of formate were reached, with the key advantage of having the unwanted acetate formation abolished [159].

5 Outlook

The global energy demand and the present high dependence on fossil fuels have caused the increase in the atmospheric CO_2 concentration for the highest values since records began. Due to its significant greenhouse effect, CO_2 rise is responsible for large and unpredictable impacts on the Earth climate, besides being responsible for ocean acidification (its major sink). While some authors defend that these alterations are no longer reversible, the CO_2 emissions must be greatly decelerate and new and more efficient "CO_2 sinks" must be developed to avoid worsen this (already huge) "carbon crisis". The three axes, storage/conversion/production, are envisaged by many authors as the best strategy to actively reduce the CO_2 emissions, while actively consuming the CO_2 already released—"two-in-one solution". Along with chemical strategies, the "biochemical way" is proving is high value in different hybrid and biological systems to convert CO_2 into fuels and VC. FDHs are efficient catalysts to reduce CO_2 to formate and are in the right way to became key partners in the longed-for safe energy/stable climate solution.

Acknowledgements This work was supported by the Associate Laboratory for Green Chemistry —LAQV, which is financed by national funds from Fundacão para a Ciência e a Tecnologia, MCTES (FCT/MCTES; UIDB/50006/2020). LBM thanks to FCT/MCTES for the CEEC-Individual 2017 Program Contract.

References

1. Friedlingstein P, Jones MW, O'Sullivan M et al (2019) Global carbon budget 2019. Earth Syst Sci Data 11:1783–1838
2. CO_2 Earth (2020). https://www.co2.earth/monthly-co2. Accessed 15 Apr 2020
3. Seixas J, Ferreira F (2020) Carbon economy and carbon footprint. In: Moura JJG, Moura I, Maia L (ed) Enzymes for solving humankind's problems, Springer Nature Switzerland AG (in press
4. Loges B, Boddien A, Junge H, Beller M (2008) Controlled generation of hydrogen from formic acid amine adducts at room temperature and application in H_2/O_2 fuel cells. Angew Chem 47:3962–3965

5. Enthaler S, Langermann J, Schmidt T (2010) Carbon dioxide and formic acid-the couple for environmental-friendly hydrogen storage? Energy Environ Sci 3:1207–1217
6. Jiang HL, Singh SK, Yan JM, Zhang XB, Xu Q (2010) Liquid-phase chemical hydrogen storage: catalytic hydrogen generation under ambient conditions. Chemsuschem 3:541–549
7. Yadav M, Xu Q (2012) Liquid-phase chemical hydrogen storage materials. Energy Environ Sci 5:9698–9725
8. Appel AM, Bercaw JE, Bocarsly AB, Dobbek H, DuBois DL, Dupuis M, Ferry JG, Fujita E, Hille R, Kenis PJA, Kerfeld CA, Morris RH, Peden CHF, Portis AR, Ragsdale SW, Rauchfuss TB, Reek JNH, Seefeldt LC, Thauer RK, Waldrop GL (2013) Frontiers, opportunities, and challenges in biochemical and chemical catalysis of CO_2 fixation. Chem Rev 113:6621–6658
9. Kuehnel MF, Wakerley DW, Orchard KL, Reisner E (2015) Photocatalytic formic acid conversion on cds nanocrystals with controllable selectivity for H_2 or CO. Angew Chem 54:9627–9631
10. Wang W, Himeda Y, Muckerman JT, Manbeck G, Fujita E (2015) CO_2 Hydrogenation to formate and methanol as an alternative to photo—and electrochemical CO_2 reduction. Chem Rev 115:12936–12973
11. Preuster P, Papp C, Wasserscheid P (2017) Liquid organic hydrogen carriers (LOHCs): toward a hydrogen-free hydrogen economy. Acc Chem Res 50:74–85
12. Sordakis K, Tang CH, Vogt LK, Junge H, Dyson PJ, Beller M, Laurenczy G (2018) Homogeneous catalysis for sustainable hydrogen storage in formic acid and alcohols. Chem Rev 118:372–433
13. Zhong H, Iguchi M, Chatterjee M, Himeda Y, Xu Q, Kawanami H (2018) Formic acid-based liquid organic hydrogen carrier system with heterogeneous catalysts. Adv Sustain Syst 2:1700161
14. Yu X, Pickup PG (2008) Recent advances in direct formic acid fuel cells (DFAFC). J Power Sources 182:124–132
15. Sahin S, Cai R, Milton RD, Abdellaoui S, Macazo FC, Minteer SD (2018) Molybdenum-dependent formate dehydrogenase for formate bioelectrocatalysis in a formate/O_2 enzymatic fuel cell. J Electrochem Soc 165:109–113
16. Yuan M, Sahin S, Cai R, Abdellaoui S, Hickey DP, Minteer SD, Milton RD (2018) Creating a low-potential redox polymer for efficient electroenzymatic CO_2 reduction. Angew Chem 57:6582–6586
17. EPFL News (2020). https://actu.epfl.ch/news/the-world-s-first-formic-acid-based-fuel-cell/. Accessed 15 Apr 2020
18. BBC News (2020). https://www.bbc.com/news/business-40403351. Accessed 15 Apr 2020
19. Bar-Even A, Noor E, Flamholz A, Milo R (2013) Design and analysis of metabolic pathways supporting formatotrophic growth for electricity-dependent cultivation of microbes. Biochim Biophys Acta 1827:1039–1047
20. Benson EE, Kubiak CP, Sathrum AJ, Smieja JM (2009) Electrocatalytic and homogeneous approaches to conversion of CO_2 to liquid fuels. Chem Soc Rev 38:89–99
21. DuBois MR, DuBois DL (2009) Development of molecular electrocatalysts for CO_2 reduction and H_2 production/oxidation. Acc Chem Res 42:1974–1982
22. Whipple DT, Kenis PJA (2010) Prospects of CO_2 utilization via direct heterogeneous electrochemical reduction. J Phys Chem Lett 1:3451–3458
23. Agarwal AS, Zhai Y, Hill D, Sridhar N (2011) The electrochemical reduction of carbon dioxide to formate/formic acid: engineering and economic feasibility. Chemsuschem 4:1301–1310
24. Schneider J, Jia HF, Muckerman JT, Fujita E (2012) Thermodynamics and kinetics of CO_2, CO, and H + binding to the metal centre of CO_2 reduction catalysts. Chem Soc Rev 41:2036–2051
25. Costentin C, Robert M, Saveant JM (2013) Catalysis of the electrochemical reduction of carbon dioxide. Chem Soc Rev 42:2423–2436

26. Jhong HR, Ma S, Kenis PJA (2013) Electrochemical conversion of CO_2 to useful chemicals: current status, remaining challenges, and future opportunities. Curr Opin Chem Eng 2:191–199
27. Clark ML, Grice KA, Moore CE, Rheingold AL, Kubiak CP (2014) Electrocatalytic CO_2 reduction by M(bpy–R) $(CO)_4$ (M = Mo, W; R = H, tBu) complexes. electrochemical, spectroscopic and computational studies and comparison with group 7 catalysts. Chem Sci 5:1894–1900
28. Kopljar D, Inan A, Vindayer P, Wagner N, Klemm E (2014) Electrochemical reduction of CO_2 to formate at high current density using gas diffusion electrodes. J Appl Electrochem 44:1107–1116
29. Lu X, Leung DY, Wang H, Leung MK, Xuan J (2014) Electrochemical reduction of carbon dioxide to formic acid. ChemElectroChem 1:836–849
30. Qiao J, Liu Y, Hong F, Zhang J (2014) A review of catalysts for the electroreduction of carbon dioxide to produce low carbon fuels. Chem Soc Rev 43(2):631–675
31. Martín AJ, Larrazábal GO, Pérez-Ramírez J (2015) Towards sustainable fuels and chemicals through the electrochemical reduction of CO_2: lessons from water electrolysis. Green Chem 17:5114–5130
32. Pletcher D (2015) The cathodic reduction of carbon dioxide—what can it realistically achieve? a mini review. Electrochem Commun 61:97–101
33. Yoo JS, Christensen R, Vegge T, Nørskov JK, Studt F (2016) Theoretical Insight into the trends that guide the electrochemical reduction of carbon dioxide to formic acid. Chemsuschem 9:358–363
34. Morris AJ, Meyer GJ, Fujita E (2009) Molecular approaches to the photocatalytic reduction of carbon dioxide for solar fuels. Acc Chem Res 42:1983–1994
35. Doherty MD, Grills DC, Muckerman JT, Polyansky DE (2010) Toward more efficient photochemical CO_2 reduction: Use of $scCO_2$ or photogenerated hydrides. Coord Chem Rev 254:2472–2482
36. Takeda H, Ishitani O (2010) Development of efficient photocatalytic systems for CO2 reduction using mononuclear and multinuclear metal complexes based on mechanistic studies. Coord Chem Rev 254:346–354
37. Tamaki Y, Morimoto T, Koike K, Ishitani O (2012) Photocatalytic CO_2 reduction with high turnover frequency and selectivity of formic acid formation using Ru(II) multinuclear complexes. Proc Natl Acad Sci U S A 109:15673–15678
38. Izumi Y (2013) Recent advances in the photocatalytic conversion of carbon dioxide to fuels with water and/or hydrogen using solar energy and beyond. Coord Chem Rev 257:171–186
39. Navalon S, Dhakshinamoorthy A, Garcia AMH (2013) Photocatalytic CO_2 reduction using non-titanium metal oxides and sulfides. Chemsuschem 6:562–577
40. Oh Y, Hu X (2013) Organic molecules as mediators and catalysts for photocatalytic and electrocatalytic CO_2 reduction. Chem Soc Rev 42:2253–2261
41. Das S, Daud WMAW (2014) Photocatalytic CO_2 transformation into fuel: a review on advances in photocatalyst and photoreactor. Renew Sustain Energy Rev 39:765–805
42. Zhou X, Liu R, Sun K, Chen Y, Verlage E, Francis SA, Lewis NS, Xiang C (2016) Solar-driven reduction of 1 atm of CO_2 to formate at 10% energy-conversion efficiency by use of a TiO_2-protected III-V tandem photoanode in conjunction with a bipolar membrane and a Pd/C cathode. ACS Energy Lett 1:764–770
43. Nocera DG (2017) Solar fuels and solar chemicals industry. Acc Chem Res 50:616–619
44. Zhang B, Sun L (2019) Artificial photosynthesis: opportunities and challenges of molecular catalysts. Chem Soc Rev 48:2216–2264
45. Graf E, Leitner W (1992) Direct formation of formic-acid from carbon-dioxide and dihydrogen using the $[(Rh(Cod)Cl)_2]Ph_2P\text{-}(CH2)_4PPh_2$ catalyst system. J Chem Soc Chem Commun 1992:623–624
46. Jessop PG, Ikariya T, Noyori R (1994) Homogeneous catalytic-hydrogenation of supercritical carbon-dioxide. Nature 368:231–233

47. Gassner F, Leitner W (1993) Hydrogenation of carbon-dioxide to formic-acid using water-soluble rhodium catalysts. J Chem Soc Chem Commun 1993:1465–1466
48. Jessop PG, Ikariya T, Noyori R (1995) Homogeneous hydrogenation of carbon-dioxide. Chem Rev 95:259–272
49. Leitner W (1995) Carbon dioxide as a raw material: synthesis of formic acid and its derivatives from CO_2. Angew Chem 34:2207–2221
50. Munshi P, Main AD, Linehan JC, Tai CC, Jessop PG (2002) Hydrogenation of carbon dioxide catalyzed by ruthenium trimethylphosphine complexes: the accelerating effect of certain alcohols and amines. J Am Chem Soc 124:7963–7971
51. Jessop PG, Joó F, Tai CC (2004) Recent advances in the homogeneous hydrogenation of carbon dioxide. Coord Chem Rev 248:2425–2442
52. Enthaler S (2008) Carbon dioxide—the hydrogen-storage material of the future? Chemsuschem 1:801–804
53. Fukuzumi S (2008) Bioinspired energy conversion systems for hydrogen production and storage. Eur J Inorg Chem 2008:1351–1362
54. Federsel C, Jackstell R, Boddien A, Laurenczy G, Beller M (2010) Ruthenium-catalyzed hydrogenation of bicarbonate in water. Chemsuschem 3:1048–1050
55. Loges B, Boddien A, Gartner F, Junge H, Beller M (2010) Catalytic generation of hydrogen from formic acid and its derivatives: useful hydrogen storage materials. Top Catal 53:902–914
56. Himeda Y, Miyazawa S, Hirose T (2011) Interconversion between formic acid and H_2/CO_2 using rhodium and ruthenium catalysts for CO_2 fixation and H_2 storage. Chemsuschem 4:487–493
57. Langer R, Diskin-Posner Y, Leitus G, Shimon LJW, Ben-David Y, Milstein D (2011) Low-pressure hydrogenation of carbon dioxide catalyzed by an iron pincer complex exhibiting noble metal activity. Angew Chem 50:9948–9952
58. Schmeier TJ, Dobereiner GE, Crabtree RH, Hazari N (2011) Secondary coordination sphere interactions facilitate the insertion step in an iridium(iii) CO_2 reduction catalyst. J Am Chem Soc 133:9274–9277
59. Wang W, Wang S, Ma X, Gong J (2011) Recent advances in catalytic hydrogenation of carbon dioxide. Chem Soc Rev 40:3703–3727
60. Hull JF, Himeda Y, Wang W-H, Hashiguchi B, Periana R, Szalda DJ, Muckerman JT, Fujita E (2012) Reversible hydrogen storage using CO_2 and a proton-switchable iridium catalyst in aqueous media under mild temperatures and pressures. Nat Chem 4:383–388
61. Maenaka Y, Suenobu T, Fukuzumi S (2012) Catalytic interconversion between hydrogen and formic acid at ambient temperature and pressure. Energy Environ Sci 5:7360–7367
62. Yadav M, Xu Q (2012) Liquid-phase chemical hydrogen storage materials Energy. Environ Sci 5:9698–9725
63. Wesselbaum S, Hintermair U, Leitner W (2012) Continuous-flow hydrogenation of carbon dioxide to pure formic acid using an integrated $scCO_2$ process with immobilized catalyst and base. Angew Chem 51:8585–8588
64. Huff CA, Sanford MS (2013) Catalytic CO_2 hydrogenation to formate by a ruthenium pincer complex. ACS Catal 3:2412–2416
65. Jeletic MS, Mock MT, Appel AM, Linehan JCA (2013) Cobalt-based catalyst for the hydrogenation of CO_2 under ambient conditions. J Am Chem Soc 135:11533–11536
66. Muller K, Sun Y, Thiel WR (2013) Ruthenium(II) phosphite complexes as catalysts for the hydrogenation of carbon dioxide. ChemCatChem 5:1340–1343
67. Wang W-H, Muckerman JT, Fujita E, Himeda Y (2013) Mechanistic insight through factors controlling effective hydrogenation of CO_2 catalyzed by bioinspired proton-responsive iridium(iii) complexes. ACS Catal 3:856–860
68. Bays JT, Priyadarshani N, Jeletic MS, Hulley EB, Miller DL, Linehan JC, Shaw WJ (2014) The influence of the second and outer coordination spheres on $Rh(diphosphine)_2$ CO_2 hydrogenation catalysts. ACS Catal 4:3663–3670

69. Filonenko GA, van Putten R, Schulpen EN, Hensen EJM, Pidko E (2014) A highly efficient reversible hydrogenation of carbon dioxide to formates using a ruthenium PNP-Pincer catalyst. ChemCatChem 6:1526–1530
70. Hsu S-F, Rommel S, Eversfield P, Muller K, Klemm E, Thiel WR, Plietker BA (2014) Rechargeable hydrogen battery based on Ru catalysis. Angew Chem 53:7074–7078
71. Moret S, Dyson PJ, Laurenczy G (2014) Direct synthesis of formic acid from carbon dioxide by hydrogenation in acidic media. Nat Commun 5:5017
72. Barelli L, Bidini G, Gallorini F, Servili S (2008) Hydrogen production through sorption-enhanced steam methane reforming and membrane technology: a review. Energy 33:554–570
73. Fihri A, Artero V, Razavet M, Baffert C, Leibl W, Fontecave M (2008) Cobaloxime-based photocatalytic devices for hydrogen production. Angew Chem 47:564–567
74. Gloaguen F, Rauchfuss TB (2009) Small molecule mimics of hydrogenases: hydrides and redox. Chem Soc Rev 38:100–108
75. Losse S, Vos JG, Rau S (2010) Catalytic hydrogen production at cobalt centres. Coord Chem Rev 254:2492–2504
76. Artero V, Chavarot-Kerlidou M, Fontecave M (2011) Splitting water with cobalt. Angew Chem 50:7238–7266
77. Kilgore UJ, Roberts JAS, Pool DH, Appel AM, Stewart MP, DuBois MR, Dougherty WG, Kassel WS, Bullock RM, DuBois DL (2011) [Ni(PPh2NC6H4X2)2]2 + complexes as electrocatalysts for H_2 production: effect of substituents, acids, and water on catalytic rates. J Am Chem Soc 133:5861–5872
78. Du P, Eisenberg R (2012) Catalysts made of earth-abundant elements (Co, Ni, Fe) for water splitting: recent progress and future challenges. Energy Environ Sci 5:6012–6021
79. Tran PD, Barber J (2012) Proton reduction to hydrogen in biological and chemical systems. Phys Chem Chem Phys 14:13772–13784
80. Wang M, Chen L, Sun LC (2012) Recent progress in electrochemical hydrogen production with earth-abundant metal complexes as catalysts. Energy Environ Sci 5:6763–6778
81. Chen WF, Iyer S, Sasaki K, Wang CH, Zhu YM, Muckerman JT, Fujita E (2013) Biomass-derived electrocatalytic composites for hydrogen evolution. Energy Environ Sci 6:1818–1826
82. Eckenhoff WT, McNamara WR, Du PW, Eisenberg R (2013) Cobalt complexes as artificial hydrogenases for the reductive side of water splitting. Biochim Biophys Acta—Bioenerg 1827:958–973
83. Thoi VS, Sun YJ, Long JR, Chang CJ (2013) Complexes of earth-abundant metals for catalytic electrochemical hydrogen generation under aqueous conditions. Chem Soc Rev 42:2388–2400
84. Faber MS, Jin S (2014) Earth-abundant inorganic electrocatalysts and their nanostructures for energy conversion applications. Energy Environ Sci 7:3519–3542
85. Liu YM, Yu HT, Quan X, Chen S, Zhao HM, Zhang YB (2014) Efficient and durable hydrogen evolution electrocatalyst based on nonmetallic nitrogen doped hexagonal carbon. Sci Rep 4:6843
86. McKone JR, Marinescu SC, Brunschwig BS, Winkler JR, Gray HB (2014) Earth-abundant hydrogen evolution electrocatalysts. Chem Sci 5:865–878
87. Pan LF, Li YH, Yang S, Liu PF, Yu MQ, Yang HG (2014) Molybdenum carbide stabilized on graphene with high electrocatalytic activity for hydrogen evolution reaction. Chem Commun 50:13135–13137
88. Xiao P, Sk MA, Thia L, Ge XM, Lim RJ, Wang JY, Lim KH, Wang X (2014) Molybdenum phosphide as an efficient electrocatalyst for the hydrogen evolution reaction. Energy Environ Sci 7:2624–2629
89. Clough AJ, Yoo JW, Mecklenburg MH, Marinescu SC (2015) Two-dimensional metal-organic surfaces for efficient hydrogen evolution from water. J Am Chem Soc 137:118–121

90. Cui W, Liu Q, Xing ZC, Asiri AM, Alamry KA, Sun X (2015) MoP nanosheets supported on biomass-derived carbon flake: One-step facile preparation and application as a novel high-active electrocatalyst toward hydrogen evolution reaction. Appl Catal B 164:144–150
91. Morozan A, Goellner V, Zitolo A, Fonda E, Donnadieu B, Jones D, Jaouen F (2015) Synergy between molybdenum nitride and gold leading to platinum-like activity for hydrogen evolution. Phys Chem Chem Phys 17:4047–4053
92. Darensbourg MY, Eduaran EL, Ding S, Lunsford AL, Pathirana KD, Ghosh P, Yang X (2020) Hydrides, carbonyls, and metal—metal bonds: organometallic chemistry control of hydrogenases. In: Moura JJG, Moura I, Maia L (eds) Enzymes for solving humankind's problems, Springer Nature Switzerland AG (in press)
93. Martins M, Pereira IAC, Pita M, De Lacey AL (2020) Biological production of hydrogen. In: Moura JJG, Moura I, Maia L (eds) Enzymes for solving humankind's problems, Springer Nature Switzerland AG (in press)
94. Grimaldi S, Schoepp-Cothenet B, Ceccaldi P, Guigliarelli B, Magalon A (2013) The prokaryotic Mo/W-bisPGD enzymes family: a catalytic workhorse in bioenergetic. Biochim Biophys Acta 1827:1048–1085
95. Hartmann T, Schwanhold N, Leimkühler S (2015) Assembly and catalysis of molybdenum or tungsten-containing formate dehydrogenases from bacteria. Biochim Biophys Acta 1854:1090–1100
96. Maia LB, Moura JJG, Moura I (2015) Molybdenum and tungsten-dependent formate dehydrogenases. J Biol Inorg Chem 20:287–309
97. Magalon A, Ceccaldi P, Schoepp-Cothenet B (2017) The Prokaryotic Mo/W-bisPGD Enzymes Family. In: Hille R, Schulzke C, Kirk M (eds) Molybdenum and tungsten enzymes: biochemistry, RSC Metallobiology Series No. 5, The Royal Society of Chemistry, Cambridge, Chap. 5, p 143–191
98. Maia LB, Moura I, Moura JJG (2017) Molybdenum and tungsten-containing formate dehydrogenases: aiming to inspire a catalyst for carbon dioxide utilization. Inorg Chim Acta 455:350–363
99. Niks D, Hille R (2018) Reductive activation of CO_2 by formate dehydrogenases. Methods Enzymol 613:277–295
100. Niks D, Hille R (2019) Molybdenum—and tungsten-containing formate dehydrogenases and formylmethanofuran dehydrogenases: structure mechanism, and cofactor insertion. Ptot Sci 28:111–122
101. Nielsen CF, Lange L, Meyer AS (2019) Classification and enzyme kinetics of formate dehydrogenases for biomanufacturing via CO_2 utilization. Biotechnol Adv 37:107408
102. Kato N (1990) Formate dehydrogenase from methylotrophic yeasts. Methods Enzymol 188:459–462
103. Vinals C, Depiereux E, Feytmans E (1993) Prediction of structurally conserved regions of D-specific hydroxy acid dehydrogenases by multiple alignment with formate dehydrogenase. Biochem Biophys Res Commun 192:182–188
104. Popov VO, Lamzin VS (1994) NAD + -dependent formate dehydrogenase. Biochem J 301:625–643
105. Filippova EV, Polyakov KM, Tikhonova TV, Stekhanova TN, Boiko KM, Popov KO (2005) Structure of a new crystal modification of the bacterial NAD-dependent formate dehydrogenase with a resolution of 2.1 Å. Crystallogr Rep 50:796–800
106. Schirwitz K, Schmidt A, Lamzin VS (2007) High resolution structures of formate dehydrogenase from Candida boidinii. Protein Sci 16:1146–1156
107. Shabalin IG, Polyakov KM, Tishkov VI, Popov VO (2009) Atomic resolution crystal structure of NAD(+)-dependent formate dehydrogenase from bacterium moraxella Sp. C-1. Acta Nat 1:89–93
108. Alekseeva AA, Savin SS, Tishkov VI (2011) NAD (+) -dependent formate dehydrogenase from plants. Acta Nat 3:38–54

109. Guo Q, Gakhar L, Wickersham K, Francis K, Vardi-Kilshtain A, Major DT, Cheatum CM, Kohen A (2016) Structural and kinetic studies of formate dehydrogenase from candida boidinii. Biochemistry 55:2760–2771
110. Hille R, Hall J, Basu P (2014) The mononuclear molybdenum enzymes. Chem Rev 114:3963–4038
111. Maia L, Moura I, Moura JJG (2017) Molybdenum and tungsten-containing enzymes: an overview. In: Hille R, Schulzke C, Kirk M (eds) Molybdenum and *Tungsten Enzymes: Biochemistry*, RSC Metallobiology Series No. 5, The Royal Society of Chemistry, Cambridge, Chap. 1, p 1–80
112. Maia L, Moura JJG (2018) Mononuclear molybdenum-containing enzymes. Reference module in chemistry, molecular sciences and chemical engineering, pp 1–19. https://doi.org/10.1016/B978-0-12-409547-2.13932-0
113. Zinoni F, Birkmann A, Stadtman TC, Böck A (1986) Nucleotide sequence and expression of the selenocysteine-containing polypeptide of formate dehydrogenase (Formate-Hydrogen-Lyase-Linked) from *Escherichia coli*. Proc Natl Acad Sci USA 83:4650–4654
114. Axley MJ, Grahame DA, Stadtman TC (1990) *Escherichia coli* formate-hydrogen Lyase. J Biol Chem 265:18213–18218
115. Gladyshev VN, Boyington JC, Khangulov SV, Grahame DA, Stadtman TC, Sun PD (1996) Characterization of crystalline formate dehydrogenase h from *Escherichia coli*. J Biol Chem 271:8095–8100
116. Boyington JC, Gladyshev VN, Khangulov SV, Stadtman T, Sun PD (1997) Crystal structure of formate dehydrogenase H: catalysis involving Mo, molybdopterin, selenocysteine and an Fe_4S_4 cluster. Science 275:1305–1308
117. Raaijmakers HCA, Romão MJ (2006) Formate-reduced E coli formate dehydrogenase H: the reinterpretation of the crystal structure suggests a new reaction mechanism. J Biol Inorg Chem 11:849–854
118. Jormakka M, Tornroth S, Abramson J, Byrne B, Iwata S (2002) Purification and crystallization of the respiratory complex formate dehydrogenase-N from *Escherichia coli*. Acta Crystallogr D Biol Crystallogr 58:160–162
119. Jormakka M, Törnroth S, Byrne B, Iwata S (2002) Molecular basis of proton motive force generation: structure of formate dehydrogenase-N. Science 2295:1863–1868
120. Wang H, Gunsalus RP (2003) Coordinate regulation of the *Escherichia coli* formate dehydrogenase fdnGHI and fdhF genes in response to nitrate, nitrite and formate: roles fro NarL and NarP. J Bacteriol 185:5076–5085
121. Pommier J, Mandrand MA, Holt SE, Boxer DH, Giodano G (1992) A second phenazine methosulphate-linked formate dehydrogenase isoenzyme in *Escherichia coli*. Biochim Biophys Acta 1107:305–313
122. Plunkett G, Burland V, Daniels DL, Blattner FR (1993) Analysis of the *Escherichia coli* genome. Nucleic Acids Res 21:3391–3398
123. Abaibou H, Pommier J, Benoit JP, Giordano G, Mandrand M (1995) Expression and characterization of the *Escherichia coli* fdo locus and a possible physiological role for aerobic formate dehydrogenase. J Bacteriol 177:7141–7149
124. Bursakov S, Liu M-Y, Payne WJ, LeGall J, Moura I, Moura JJG (1995) Isolation and preliminary characterization of a soluble nitrate reductase from the sulfate reducing organism *Desulfovibrio desulfuricans* ATCC 27774. Anaerobe 1:55–60
125. Sebban C, Blanchard L, Bruschi M, Guerlesquin F (1995) Purification and characterization of the formate dehydrogenase from *Desulfovibrio vulgaris* hildenborough. FEMS Microbiol Lett 133:143–149
126. Brondino CD, Passeggi MCG, Caldeira J, Almendra MJ, Feio MJ, Moura JJG, Moura I (2004) Incorporation of either molybdenum or tungsten into formate dehydrogenase from *Desulfovibrio alaskensis* NCIMB 13491. J Biol Inorg Chem 9:145–151

127. Heidelberg JF, Seshadri R, Haveman SA, Hemme CL, Paulsen IT, Kolonay JF, Eisen JA, Ward N, Methe B, Brinkac LM, Daugherty SC, Deboy RT, Dodson RJ, Durkin AS, Madupu R, Nelson WC, Sullivan SA, Fouts D, Haft DH, Selengut J, Peterson JD, Davidsen TM, Zafar N, Zhou L, Radune D, Dimitrov G, Hance M, Tran K, Khouri H, Gill J, Utterback TR, Feldblyum TV, Wall JD, Voordouw G, Fraser CM (2004) The genome sequence of the anaerobic, sulfate-reducing bacterium *Desulfovibrio vulgaris* hildenborough. Nat Biotechnol 22:554–559
128. Mota CS, Valette O, Gonzalez PJ, Brondino CD, Moura JJG, Moura I, Dolla A, Rivas MG (2011) Effects of molybdate and tungstate on expression levels and biochemical characteristics of formate dehydrogenases produced by *Desulfovibrio alaskensis* NCIMB 13491. J Bacteriol 193:2917–2923
129. Silva SM, Pimentel C, Valente FMA, Rodrigues-Pousada C, Pereira IAC (2011) Tungsten and molybdenum regulation of formate dehydrogenase expression in *Desulfovibrio vulgaris* hildenborough. J Bacteriol 193:2908–2916
130. Raaijmakers H, Macieira S, Dias JM, Texierira S, Bursakov S, Huber R, Moura JJG, Moura I, Romão MJ (2002) Gene sequence and the 18Å crystal structure of the tungsten-containing formate dehydrogenase from *Desulfovibrio gigas*. Structure 10:1261–1272
131. da Silva SM, Voordouw J, Leitão C, Martins M, Voordouw G, Pereira IAC (2013) Function of formate dehydrogenases in *Desulfovibrio vulgaris* hildenborough energy metabolism. Microbiology 159:1760–1769
132. Oliveira AR, Mota C, Mourato C, Domingos RM, Santos MFA, Gesto D, Guigliarelli B, Santos-Silva T, Romão MJ, Pereira IAC (2020) Toward the mechanistic understanding of enzymatic CO_2 reduction. ACS Catal 10:3844–3856
133. Almendra MJ, Brondino CD, Gavel O, Pereira AS, Tavares P, Bursakov S, Duarte R, Caldeira J, Moura JJ, Moura I (1999) Purification and characterization of a tungsten-containing formate dehydrogenase from *Desulfovibrio gigas*. Biochemistry 38:16366–16372
134. Raaijmakers H, Teixeira S, Dias JM, Almendra MJ, Brondino CD, Moura I, Moura JJ, Romão MJ (2001) Tungsten-containing formate dehydrogenase from *Desulfovibrio gigas*: metal identification and preliminary structural data by multi-wavelength crystallography. J Biol Inorg Chem 6:398–404
135. Costa C, Teixeira M, LeGall J, Moura JJG, Moura I (1997) Formate dehydrogenase from *Desulfovibrio desulfuricans* ATCC 27774: isolation and spectroscopic characterization of the active sites. J Biol Inorg Chem 2:198–208
136. Rivas M, Gonzalez P, Brondino CD, Moura JJG, Moura I (2007) EPR characterization of the molybdenum(V) forms of formate dehydrogenase from *Desulfovibrio desulfuricans* ATCC 27774 upon formate reduction. J Inorg Biol 101:1617–1622
137. Maia L, Fonseca L, Moura I, Moura JJG (2016) Reduction of carbon dioxide by a molybdenum-containing formate dehydrogenase: a kinetic and mechanistic study. J Am Chem Soc 138:8834–8846
138. Young T, Niks D, Hakopian S, Tam TK, Yu X, Hille R, Blaha GM (2020) Crystallographic and kinetic analyses of the FdsBG subcomplex of the cytosolic formate dehydrogenase FdsABG from *Cupriavidus necator*. J Biol Chem 295:6570–6585
139. Radon C, Mittelstädt G, Duffus BR, Bürger J, Hartmann T, Mielke T, Teutloff C, Leimkühler S, Wendler P (2020) Cryo-EM structures reveal intricate Fe-S cluster arrangement and charging in *Rhodobacter capsulatus* formate dehydrogenase. Nat Commun 11:1912
140. Wagner T, Ermler U, Shima S (2016) The methanogenic CO2 reducing-and-fixing enzyme is bifunctional and contains 46 [4Fe-4S] clusters. Science 354:114–117
141. Trchounian K, Poladyan A, Vassilian A, Trchounian A (2012) Multiple and reversible hydrogenases for hydrogen production by *Escherichia coli*. Crit Rev Biochem Mol Biol 47:236–249

142. Babujee L, Apodaca J, Balakrishnan V, Liss P, Kiley PJ, Charkowski AO, Glasner JD, Perna NT (2012) Evolution of the metabolic and regulatory networks associated with oxygen availability in two phytopathogenic enterobacteria. BMC Genom 13:110
143. Liou JS-C, Balkwill DL, Drake GR, Tanner RS (2005) Clostridium carboxidivorans Sp. Nov., a solvent-producing clostridium isolated from an agricultural settling lagoon, and reclassification of the acetogen clostridium scatologenes strain SL1 as clostridium drakei Sp Nov. Int J Syst Evol Microbiol 55:2085–2091
144. Ragsdale SW, Pierce E (2008) Acetogenesis and the wood-Ljungdahl pathway of CO_2 fixation. Biochim Biophys Acta 1784:1873–1898
145. Bruant G, Levesque M-J, Peter C, Guiot SR, Masson L (2010) Genomic analysis of carbon monoxide utilization and butanol production by clostridium carboxidivorans strain P7T. PLoS One 5:e13033
146. Paul D, Austin FW, Arick T, Bridges SM, Burgess SC, Dandass YS, Lawrence ML (2010) Genome sequence of the solvent-producing bacterium clostridium carboxidivorans strain P7T. J Bacteriol 192:5554–5555
147. Alissandratos A, Kim HK, Matthews HK, Hennessey JE, Philbrook A, Easton CJ (2013) Clostridium carboxidovorans strain P7T recombinant formate dehydrogenase catalyzes reduction of CO_2 to formate. Appl Environ Micorobiol 79:741–744
148. Bagramyan K, Trchounian A (2003) Structural and functional features of formate hydrogen lyase, an enzyme of mixed-acid fermentation from *Escherichia coli*. Biochem Moscow 68:1159–1170
149. McDowall JS, Murphy BJ, Haumann M, Palmer T, Armstrong FA, Sargent F (2014) Bacterial formate hydrogenlyase complex. Proc Natl Acad Sci U S A 111:E3948–E3956
150. Mcdowall JS, Hjersing MC, Palmer T, Sargent F (2015) Dissection and engineering of the *Escherichia coli* formate hydrogenlyase complex. FEBS Lett 589:3141–3147
151. Pinske C, Sargent F (2016) Exploring the directionality of *Escherichia coli* formate hydrogenlyase: a membrane-bound enzyme capable of fixing carbon dioxide to organic acid. MicrobiologyOpen 5:721–737
152. Litty D, Müller V (2020) Acetogenic bacteria for biotechnological applications. In: Moura JJG, Moura I, Maia L (eds) Enzymes for solving humankind's problems, Springer Nature Switzerland AG (in press)
153. Schuchmann K, Müller V (2013) Direct and reversible hydrogenation of CO2 to formate by a bacterial carbon dioxide reductase. Science 342:1382–1385
154. Schuchmann K, Vonck J, Müller V (2016) A bacterial hydrogen-dependent CO_2 reductase forms filamentous structures. FEBS J 283:1311–1322
155. Kottenhahn P, Schuchmann K, Müller V (2018) Efficient whole cell biocatalyst for formate-based hydrogen production. Biotechnol Biofuels 11:93
156. Schwarz FM, Schuchmann K, Müller V (2018) Hydrogenation of CO_2 at ambient pressure catalyzed by a highly active thermostable biocatalyst. Biotechnol Biofuels 11:237
157. Müller V (2019) New horizons in acetogenic conversion of one-carbon substrates and biological hydrogen storage. Trends Biotechnol 37:1344–1354
158. Schoelmerich MC, Müller V (2019) Energy conservation by a hydrogenase-dependent chemiosmotic mechanism in an ancient metabolic pathway. Proc Natl Acad Sci USA 116:6329–6334
159. Schwarz FM, Müller V (2020) Whole-cell biocatalysis for hydrogen storage and syngas conversion to formate using a thermophilic acetogen. Biotechnol Biofuels 13:32
160. Bertram PA, Karrasch M, Schmitz RA, Böcher R, Albracht SPJ, Thauer RK (1994) Formylmethanofuran dehydrogenases from methanogenic Archaea Substrate specificity, EPR properties and reversible inactivation by cyanide of the molybdenum or tungsten iron-sulfur proteins. Eur J Biochem 220:477–484
161. Hochheimer A, Hedderich R, Thauer RK (1998) The formylmethanofuran dehydrogenase isozymes in Methanobacterium wolfeii and Methanobacterium terhmoautotrophicum:

induction of the molybdenum isozyme by molybdate and constitutive synthesis of the tungsten isozyme. Arch Microbiol 170:389–393
162. Hille R (1996) The mononuclear molybdenum enzymes. Chem Rev 96:27575–27816
163. Johnson MK, Rees DC, Adams MWW (1996) Tungstoenzymes Chem Rev 96:2817–2839
164. Bevers LE, Hagedoorn PL, Hagen WR (2009) The bioinorganic chemistry of tungsten. Coord Chem Rev 253:269–290
165. Hagen WR (2017) Tungsten-containing enzymes. In: Hille R, Schulzke C, Kirk M (eds) Molybdenum and tungsten enzymes: biochemistry, RSC Metallobiology Series No. 5, The Royal Society of Chemistry, Cambridge, Chap 10, pp 313–342
166. Khangulov SVV, Gladyshev VN, Dismukes GC, Stadtman TC (1998) Selenium-containing formate dehydrogenase H from *Escherichia coli*: a molybdenum enzyme that catalyzes formate oxidation without oxygen transfer. Biochemistry 37:3518–3528
167. Thome R, Gust A, Toci R, Mendel R, Bittner F, Magalon A, Walburger A (2012) A sulfurtransferase is essential for activity of formate dehydrogenases in *Escherichia coli*. J Biol Chem 287:4671–4678
168. Arnoux P, Ruppelt C, Oudouhou F, Lavergne J, Siponen MI, Toci R, Mendel RR, Bittner F, Pignol D, Magalon A, Walburger A (2015) Sulphur shuttling across a chaperone during molybdenum cofactor maturation. Nat Commun 6:6148
169. Schrapers P, Hartmann T, Kositzki R, Dau H, Reshke S, Schulzke C, Leimkühler S, Haumann M (2015) Sulfido and cysteine ligation changes at the molybdenum cofactor during substrate conversion by formate dehydrogenase (FDH) from *Rhodobacter capsulatus*. Inorg Chem 54:3260–3271
170. Blanchard JS, Cleland WW (1980) Kinetic and chemical mechanisms of yeast formate dehydrogenase. Biochemistry 19:3543–3550
171. Rotberg NS, Cleland WW (1991) Secondary 15 N isotope effects on the reactions catalyzed by alcohol and formate dehydrogenases. Biochemistry 30:4068–4071
172. Lamzin VS, Dauter Z, Popov VO, Harutyunyan EH, Wilson KS (1994) High resolution structures of holo and apo formate dehydrogenase. J Mol Biol 236:759–785
173. Tishkov VI, Matorin AD, Rojkova AM, Fedorchuk VV, Savitsky PA, Dementieva LA, Lamzin VS, Mezentzev AV, Popov VO (1996) Site-directed mutagenesis of the formate dehydrogenase active centre: role of the His332-Gln313 pair in enzyme catalysis. FEBS Lett 390:104–108
174. Mesentsev AV, Lamzin VS, Tishkov VI, Ustinnikova TB, Popov VO (1997) Effect of pH on kinetic parameters of NAD + -dependent formate dehydrogenase. Biochem J 321:475–480
175. Tishkov VI, Popov VO (2004) Catalytic mechanism and application of formate dehydrogenase. Biochemistry (Mosc) 69:1252–1267
176. Castillo R, Oliva M, Marti S, Moliner V (2008) A theoretical study of the catalytic mechanism of formate dehydrogenase. J Phys Chem B 112:10012–10022
177. Bandaria JN, Cheatum CM, Kohen A (2009) Examination of enzymatic H-tunneling through kinetics and dynamics. J Am Chem Soc 131:10151–10155
178. Nilov DK, Shabalin IG, Popov VO, Svedas VK (2012) Molecular modeling of formate dehydrogenase: the formation of the Michaelis complex. J Biomol Struct Dyn 30:170–199
179. Leopoldini M, Chiodo SG, Toscano M, Russo N (2008) Reaction mechanism of molybdoenzyme formate dehydrogenase. Chemistry 14:8674–8681
180. Mota CS, Rivas MG, Brondino CD, Moura I, Moura JJG, Gonzalez PG, Cerqueira NMFSA (2011) The mechanism of formate oxidation by metal-dependent formate dehydrogenases. J Biol Inorg Chem 16:1255–1268
181. Tiberti M, Papaleo E, Russo N, Gioia L, Zampella G (2012) Evidence for the formation of a Mo-H intermediate in the catalytic cycle of formate dehydrogenase. Inorg Chem 51:8331–8339
182. Hartmann T, Leimkuhler S (2013) The oxygen-tolerant and NAD + -dependent formate dehydrogenase from *Rhodobacter capsulatus* is able to catalyze the reduction of CO_2 to formate. FEBS J 280:6083–6096

183. Hartmann T, Schrapers P, Utesch T, Nimtz M, Rippers Y, Dau H, Mroginski MA, Haumann M, Leimkühler S (2016) The molybdenum active site of formate dehydrogenase is capable of catalyzing C-H bond cleavage and oxygen atom transfer reactions. Biochemistry 55:2381–2389
184. Niks D, Duvvuru J, Escalona M, Hille R (2016) Spectroscopic and kinetic properties of the molybdenum-containing, NAD + -dependent formate dehydrogenase from *Ralstonia eutropha*. J Biol Chem 291:1162–1174
185. Dong G, Ryde U (2018) Reaction mechanism of formate dehydrogenase studied by computational methods. J Biol Inorg Chem 23:1243–1255
186. Thauer RK, Kaufer B, Fuchs G (1975) The active species of 'CO_2' utilized by reduced ferredoxin: CO_2 oxidoreductase from clostridium pasteurianum. Eur J Biochem 55:111–117
187. Arnoux P, Sabaty M, Alric J, Frangioni B, Guigliarelli B, Adriano JM, Pignol D (2003) Structural and redox plasticity in the heterodimeric periplasmic nitrate reductase. Nat Struct Biol 10:928–934
188. Tanaka R, Yamashita M, Nozaki K (2009) Catalytic hydrogenation of carbon dioxide using Ir(III)-pincer complexes. J Am Chem Soc 131:14168–14169
189. Ziebart C, Federsel C, Anbarasan P, Jackstell R, Baumann W, Spannenberg A, Beller M (2012) Well-defined iron catalyst for improved hydrogenation of carbon dioxide and bicarbonate. J Am Chem Soc 134:20701–20704
190. Filonenko GA, Hensen EJM, Pidko EA (2014) Mechanism of CO_2 hydrogenation to formates by homogeneous Ru-PNP pincer catalyst: from a theoretical description to performance optimization. Catal Sci Technol 4:3474–3485
191. Maiti BK, Maia LB, Pal K, Pakhira B, Avilés T, Moura I, Pauleta SR, Nuñez JL, Rizzi AC, Brondino CD, Sarkar S, Moura JJG (2014) One electron reduced square planar bis (benzene-1,2-dithiolato) copper dianionic complex and redox switch by O_2/HO−. Inorg Chem 53:12799–12808
192. Lothrop AP, Snider GW, Flemer S, Ruggles EL, Davidson RS, Lamb AL, Hondal RJ (2014) Compensating for the absence of selenocysteine in high-molecular weight thioredoxin reductases: the electrophilic activation hypothesis. Biochemistry 53:664–674
193. Massey V, Edmondson D (1970) On the mechanism of inactivation of xanthine oxidase by cyanide. J Biol Chem 245:6595–6598
194. Edmondson DE, Ballou D, Vanheuvelen A, Palmer G, Massey V (1973) Kinetic studies on the substrate reduction of xanthine oxidase. J Biol Chem 248:6135–6144
195. Olson JS, Ballou DP, Palmer G, Massey V (1974) The mechanism of action of xanthine oxidase. J Biol Chem 249:4363–4382
196. Gutteridge S, Tanner SJ, Bray RC (1978) The molybdenum centre of native xanthine oxidase. evidence for proton transfer from substrates to the centre and for existence of an anion-binding site. Biochem J 175:869–878
197. Gutteridge S, Tanner SJ, Bray RC (1978) Comparison of the molybdenum centres of native and desulpho xanthine oxidase. the nature of the cyanide-labile sulphur atom and the nature of the proton-accepting group. Biochem J 175:887–897
198. Bray RC, Gutteridge S, Stotter DA, Tanner SJ (1979) The mechanism of xanthine oxidase The relationship between the rapid and very rapid electron-paramagnetic-resonance signals. Biochem J 177:357–360
199. Coughlan MP, Johnson JL, Rajagopalan KV (1980) Mechanisms of inactivation of molybdoenzymes by cyanide. J Biol Chem 255:2694–2699
200. Gutteridg S, Bray RC (1980) Oxygen-17 splitting of the very rapid molybdenum(V) e.p.r. signal from xanthine oxidase. rate of exchange with water of the coupled oxygen atom. Biochem J 189:615–623
201. Malthouse JPG, Gutteridge S, Bray RC (1980) Rapid type 2 molybdenum(V) electron-paramagnetic resonance signals from xanthine oxidase and the structure of the active centre of the enzyme. Biochem J 185:767–770

202. Xia M, Dempski R, Hille R (1999) The reductive half-reaction of xanthine oxidase Reaction with aldehydes and identification of the catalytically labile oxygen. J Biol Chem 274:3323–3330
203. Boll M (2005) Key enzymes in the anaerobic aromatic metabolism catalysing birch-like reductions. Biochim Biophys Acta 1707:34–50
204. Johannes J, Unciuleac M, Friedrich T, Warkentin E, Ermler U, Boll M (2008) Inhibitors of the molybdenum cofactor containing 4-hydroxybenzoyl-CoA reductase. Biochemistry 47:4964–4972
205. Stiefel EI (1973) Proposed molecular mechanism for the action of molybedenum in enzymes: coupled proton and electron transfer. Proc Natl Acad Sci USA 70:988–992
206. Stiefel EI (1977) The coordination and bioinorganic chemistry of molybdenum Prog. Inorg Chem 22:1–223
207. Rajapakshe A, Snyder RA, Astashkin AV, Bernardson P, Evans DJ, Young CG, Evans DH, Enemark JH (2009) Insights into the nature of Mo(V) species in solution: modeling catalytic cycles for molybdenum enzymes. Inorg Chim Acta 362:4603–4608
208. Maia L, Moura I, Moura JJG (2017) EPR spectroscopy on mononuclear molybdenum-containing enzymes. In: Hanson G, Berliner LJ (eds) Future directions in metalloprotein and metalloenzyme research, Biological Magnetic Resonance, vol 33. Springer International Publishing, Cham, Chap 4, pp 55–101
209. Wilson GL, Greenwood RJ, Pilbrow JR, Spence JT, Wedd AG (1991) Molybdenum(V) sites in xanthine oxidase and relevant analogue complexes: comparison of molybdenum-95 and sulfur-33 coupling. J Am Chem Soc 113:6803–6812
210. Duffus BR, Schrapers P, Schuth N, Mebs S, Dau H, Leimkühler S, Haumann M (2020) Anion binding and oxidative modification at the molybdenum cofactor of formate dehydrogenase from *Rhodobacter capsulatus* studied by X-ray absorption spectroscopy. Inorg Chem 59:214–225
211. Barber MJ, May HD, Ferry JG (1986) Inactivation of formate dehydrogenase from methanobacterium formicicum by cyanide? Biochemistry 25(1986):8150–8155
212. Friedebold J, Bowien B (1993) Physiological and biochemical characterization of the soluble formate dehydrogenase, a molybdoenzyme from *Alcaligenes eutrophus*. J Bacteriol 175:4719–4728
213. George GN, Colangelo CM, Dong J, Scott RA, Khangulov SV, Gladyshev VN, Stadtman TC (1998) X-ray absorption spectroscopy of the molybdenum site of *Escherichia coli* formate dehydrogenase. J Am Chem Soc 120:1267–1273
214. George GN, Costa C, Moura JJG, Moura I (1999) Observation of ligand-based redox chemistry at the active site of a molybdenum enzyme. J Am Chem Soc 121:2625–2626
215. Mota CS (2011) Faculdade de Ciências e Tecnologia, Universidade Nova de Lisboa, Portugal, PhD Thesis. https://hdl.handle.net/10362/6688
216. Axley MJ, Böck A, Stadtman TC (1991) Catalytic properties of an *Escherichia coli* formate dehydrogenase in which sulfur replaces selenium. Proc Natl Acad Sci USA 88:8450–8454
217. Coelho C, Gonzalez PJ, Moura JG, Moura I, Trincao J, Joao Romao M (2011) The crystal structure of *Cupriavidus necator* nitrate reductase in oxidized and partially reduced states. J Mol Biol 408:932–948
218. Cerqueira NMFSA, Fernandes PA, Gonsalez PJ, Moura JJG, Ramos MJ (2013) The sulfur shift: an activation mechanism for periplasmic nitrate reductase and formate dehydrogenase. Inorg Chem 52:10766–10772
219. Robinson WE, Bassegoda A, Reisner E, Hirst J (2017) Oxidation-state-dependent binding properties of the active site in a mo-containing formate dehydrogenase. J Am Chem Soc 139:9927–9936
220. Cornish-Bowden A (1995) Fundamentals of enzyme kinetics. Portland Press, London
221. Silveira CM, Almeida MG (2013) Small electron-transfer proteins as mediators in enzymatic electrochemical biosensors. Anal Bioanal Chem 405:3619–3635

222. Armstrong FA, Hirst J (2011) Reversibility and efficiency in electrocatalytic energy conversion and lessons from enzymes. Proc Natl Acad Sci U S A 108:14049–14054
223. Fourmond V, Léger C (2016) Protein electrochemistry: questions and answers. In: Jeuken L (ed) Biophotoelectrochemistry: from bioelectrochemistry to biophotovoltaics. Advances in biochemical engineering/biotechnology, vol 158. Springer, Cham
224. Fourmond V, Léger C (2017) Modelling the voltammetry of adsorbed enzymes and molecular catalysts. Curr Opin Electrochem 1:110–120
225. Fourmond V (2017) Direct Electrochemistry of molybdenum and tungsten enzymes. Reference module in chemistry, molecular sciences and chemical engineering, pp 477–488 https://doi.org/10.1016/B978-0-12-409547-2.13354-2
226. Li H, Buesen D, Dementin S, Léger C, Fourmond V, Plumeré N (2019) Complete protection of O_2-sensitive catalysts in thin films. J Am Chem Soc 141:16734–16742
227. Fourmond V, Wiedner ES, Shaw WJ, Léger C (2019) Understanding and design of bidirectional and reversible catalysts of multielectron, multistep reactions. J Am ChemSoc 141:11269–11285
228. Kornienko N, Zhang JZ, Sakimoto KK, Yang P, Reisner E (2018) Semi-artificial photosynthesis: interfacing nature's catalytic machinery with synthetic materials. Nat Nanotechnol 13:890
229. Bok FA, Hagedoorn PL, Silva PJ, Hagen WR, Schiltz E, Fritsche K, Stams AJ (2003) Two W-containing Formate Dehydrogenases (CO_2-reductases) involved in syntrophic propionate oxidation by syntrophobacter fumaroxidans. Eur J Biochem 270:2476–2485
230. Bok FA, Hagedoorn PL, Silva PJ, Hagen WR, Schiltz E, Fritsche K, Stams AJ (2003) Two W-containing formate dehydrogenases (CO_2-reductases) involved in syntrophic propionate oxidation by syntrophobacter fumaroxidans. FEBS J 270:2476–2485
231. Worm P, Stams AJ, Cheng X, Plugge CM (2011) Growth- and substrate-dependent transcription of formate dehydrogenase and hydrogenase coding genes in Syntrophobacter fumaroxidans and Methanospirillum hungatei. Microbiology 157:280–289
232. Reda T, Plugge CM, Abram NJ, Hirst J (2008) Reversible interconversion of carbon dioxide and formate by an electroactive enzyme. Proc Natl Acad Sci USA 105:10654–10658
233. Kuwabata S, Tsuda R, Nishida K, Yoneyama H (1993) Electrochemical conversion of carbon dioxide to methanol with use of enzymes as biocatalysts. Chem Lett 22:1631–1634
234. Kuwabata S, Tsuda R, Yoneyama H (1994) Electrochemical conversion of carbon dioxide to methanol with the assistance of formate dehydrogenase and methanol dehydrogenase as biocatalysts. J Am Chem Soc 116:5437–5443
235. Miyatani R, Amao Y (2002) Bio-CO_2 fixation with formate dehydrogenase from saccharomyces cerevisiae and water-soluble zinc porphyrin by visible light. Biotechnol Lett 24:1931–1934
236. Tsujisho I, Toyoda M, Amao Y (2006) Photochemical and enzymatic synthesis of formic acid from CO_2 with chlorophyll and dehydrogenase. System Catal Commun 7:173–176
237. Ihara M, Kawano Y, Urano M, Okabe A (2013) Light driven CO_2 fixation by using cyanobacterial photosystem I and NADPH-dependent formate dehydrogenase. PLoS ONE 8: e71581
238. Amao Y, Shuto N (2014) Formate dehydrogenase-viologen-Immobilized Electrode for CO_2 conversion, for development of an artificial photosynthesis system. Res Chem Intermed 40:3267–3276
239. Amao Y, Takahara S, Sakai Y (2014) Visible-light induced hydrogen and formic acid production from biomass and carbon dioxide with enzymatic and artificial photosynthesis system. Int J Hydrogen Energy 39:20771–20776
240. Kim S, Kim MK, Lee SH, Yoon S, Jung KD (2014) Conversion of CO_2 to formate in an electroenzymatic cell using candida boidinii formate dehydrogenase. J Mol Catal B Enzym 102:9–15

241. Srikanth S, Maesen M, Dominguez-Benetton X, Vanbroekhoven K, Pant D (2014) Enzymatic electrosynthesis of formate through CO_2 sequestration/reduction in a bioelectrochemical system (BES). Bioresour Technol 165:350–354
242. Hwang H, Yeon YJ, Lee S, Choe H, Jang MG, Cho DH, Park S, Kim YH (2015) Electro-biocatalytic production of formate from carbon dioxide using an oxygen-stable whole cell biocatalyst. Bioresour Technol 185:35–39
243. Kim SH, Chung GY, Kim SH, Vinothkumar G, Yoon SH, Jung KD (2016) Electrochemical NADH regeneration and electroenzymatic CO_2 reduction on cu nanorods/glassy carbon electrode prepared by cyclic deposition. Electrochim Acta 210:837–845
244. Lee SY, Lim SY, Seo D, Lee JY, Chung TD (2016) Light-driven highly selective conversion of CO_2 to formate by electrosynthesized enzyme/cofactor thin film electrode. Adv Energy Mater 6:1502207
245. Nam DH, Kuk SK, Choe H, Lee S, Ko JW, Son EJ, Choi EG, Kim YH, Park CB (2016) Enzymatic photosynthesis of formate from carbon dioxide coupled with highly efficient photoelectrochemical regeneration of nicotinamide cofactors. Green Chem 18:5989–5993
246. Schlager S, Dumitru LM, Haberbauer M, Fuchsbauer A, Neugebauer H, Hiemetsberger D, Wagner A, Portenkirchner E, Sariciftci NS (2016) Electrochemical reduction of carbon dioxide to methanol by direct injection of electrons into immobilized enzymes on a modified electrode. Chemsuschem 9:631–635
247. Ikeyama S, Amao Y (2017) A Novel electron carrier molecule based on a viologen derivative for visible light-driven CO_2 reduction to formic acid with the system of zinc porphyrin and formate dehydrogenase. Sustain Energy Fuels 1:1730–1733
248. Noji T, Jin T, Nango M, Kamiya N, Amao Y (2017) CO_2 photoreduction by formate dehydrogenase and a Ru-complex in a nanoporous glass reactor. ACS Appl Mater Interfaces 9:3260–3265
249. Zhang L, Liu J, Ong J, Li SFY (2016) Specific and sustainable bioelectro-reduction of carbon dioxide to formate on a novel enzymatic cathode. Chemosphere 162:228–234
250. Yadav RK, Baeg J-O, Oh GH, Park N-J, Kong K-J, Kim J, Hwang DW, Biswas SK (2012) A photocatalyst-enzyme coupled artificial photosynthesis system for solar energy in production of formic acid from CO_2. J Am Chem Soc 134:11455–11461
251. El-Zahab B, Donnelly D, Wang P (2008) Particle-tethered NADH for production of methanol from CO_2 catalyzed by coimmobilized enzymes. Biotechnol Bioeng 99:508–514
252. Choe H, Joo JC, Cho DH, Kim MH, Lee SH, Jung KD, Kim YH (2014) Efficient CO_2-reducing activity of NAD-dependent formate dehydrogenase from thiobacillus sp KNK65MA for formate production from CO_2 gas. PLoS ONE 9:e103111
253. Kuk SK, Singh RK, Nam DH, Singh R, Lee JK, Park CB (2017) Photoelectrochemical reduction of carbon dioxide to methanol through a highly efficient enzyme cascade. Angew Chem 56:3827–3832
254. Sakai K, Kitazumi Y, Shirai O, Kano K (2016) Bioelectrocatalytic formate oxidation and carbon dioxide reduction at high current density and low overpotential with tungsten-containing formate dehydrogenase and mediators. Electrochem Commun 65:31–34
255. Sakai K, Kitazumi Y, Shirai O, Takagi K, Kano K (2016) Efficient bioelectrocatalytic CO_2 reduction on gas-diffusion-type biocathode with tungsten-containing formate dehydrogenase. Electrochem Commun 73:85–88
256. Sakai K, Kitazumi Y, Shirai O, Takagi K, Kano K (2017) direct electron transfer-type four-way bioelectrocatalysis of CO_2/ formate and NAD +/NADH redox couples by tungsten-containing formate dehydrogenase adsorbed on gold nanoparticle-embedded mesoporous carbon electrodes modified with 4-Mercaptopyridine. Electrochem Commun 84:75–79
257. Sakai K, Sugimoto Y, Kitazumi Y, Shirai O, Takagi K, Kano K (2017) Direct electron transfer-type bioelectrocatalytic interconversion of carbon dioxide/formate and NAD +/NADH redox couples with tungsten-containing formate dehydrogenase. Electrochim Acta 228:537–544

258. Sakai K, Xia H, Kitazumi Y, Shirai O, Kano K (2018) Assembly of direct-electron-transfer-type bioelectrodes with high performance. Electrochim Acta 271:305–311
259. Muller U, Willnow P, Ruschig U, Hopner T (1978) Formate dehydrogenase from *Pseudomonas oxalaticus*. Eur J Biochem 83:485–498
260. Yu X, Niks D, Mulchandani A, Hille R (2017) Efficient reduction of CO_2 by the molybdenum-containing formate dehydrogenase from *Cupriavidus necator* (*Ralstonia eutropha*). J Biol Chem 292:16872–16879
261. Walker LM, Li V, Niks D, Hille R, Elliott SJ (2019) Deconvolution of reduction potentials of formate dehydrogenase from *Cupriavidus necator*. J Biol Inorg Chem 24:889–898
262. Yu X, Niks D, Ge X, Liu H, Hille R, Mulchandani A (2019) Synthesis of formate from CO_2 gas catalyzed by an O_2-tolerant NAD-dependent formate dehydrogenase and glucose dehydrogenase. Biochemistry 58:1861–1868
263. Bassegoda A, Madden C, Wakerley DW, Reisner E, Hirst J (2014) Reversible interconversion of CO_2 and formate by a molybdenum-containing formate dehydrogenase. J Am Chem Soc 136:15473–15476
264. Roger M, Brown F, Gabrielli W, Sargent F (2018) Efficient hydrogen-dependent carbon dioxide reduction by *Escherichia coli*. Curr Biol 28:140–145
265. Singh S, Noori MT, Verm N (2020) Efficient bio-electroreduction of CO_2 to formate on a iron phthalocyanine-dispersed CDC in microbial electrolysis system. ElectrochimActa 338:135887
266. Cordas CM, Campaniço M, Baptista R, Maia LB, Moura I, Moura JJG (2019) Direct electrochemical reduction of carbon dioxide by a molybdenum-containing formate dehydrogenase. J Inorg Biochem 196:110694
267. Mourato C, Martins M, da Silva SM, Pereira IA (2017) A continuous system for biocatalytic hydrogenation of CO_2 to Formate. Bioresour Technol 235:149–156
268. Martins M, Mourato C, Pereira IAC (2015) *Desulfovibrio vulgaris* growth coupled to formate-driven H_2 production. Environ Sci Technol 49:14655–14662
269. Martins M, Mourato C, Morais-Silva FO, Rodrigues- Pousada C, Voordouw G, Wall JD, Pereira IAC (2016) Electron transfer pathways of formate-driven H_2 production in Desulfovibrio. Appl Microbiol Biotechnol 100:8135–8146
270. Sokol KP, Robinson WE, Oliveira AO, Warnan J, Nowaczyk MM, Ruff A, Pereira IAC, Reisner E (2018) Photoreduction of CO_2 with a formate dehydrogenase driven by photosystem II using a semi-artificial Z-scheme architecture. J Am Chem Soc 140:16418–16422
271. Miller M, Robinson WR, Oliveira AR, Heidary N, Kornienko N, Warnan J, Pereira IAC, Reisner E (2019) Interfacing formate dehydrogenase with metal oxides for the reversible electrocatalysis and solar-driven reduction of carbon dioxide. Angew Chem 58:4601–4605
272. Szczesny J, Ruff A, Oliveira AR, Pita M, Pereira IAC, De Lacey AL, Schuhmann W (2020) Electroenzymatic CO_2 fixation using redox polymer/enzyme-modified gas diffusion electrodes. ACS Energy Lett 5:321–327
273. Sokol KP, Robinson WE, Oliveira AR, Zacarias S, Lee C-Y, Madden C, Bassegoda A, Hirst J, Pereira IAC, Reisner E (2019) Reversible and selective interconversion of hydrogen and carbon dioxide into formate by a semiartificial formate hydrogenlyase mimic. J Chem Am Soc 141:17498–17502
274. Berg IA, Kockelkorn D, Ramos-Vera WH, Say RF, Zarzycki J, Hügler M (2010) Autotrophic carbon fixation in archaea. Nat Rev Microbiol 8:447–460
275. Martin WF, Thauer RK (2017) Energy in ancient metabolism. Cell 168:953–955